Fractionated Radiation Severely Reduces the Number of CD8+ T Cells and Mature Antigen Presenting Cells Within Lung Tumors

Reijmen, Eva; De Mey, Sven; De Mey, Wout; Gevaert, Thierry; De Ridder, Kirsten; Locy, Hanne; Martens, Sandrina; De Blay, Emmy; Bouwens, Luc; Debie, Pieterjan; Breckpot, Karine; De Grève, Jacques; De Ridder, Mark; Goyvaerts, Cleo

Published in:
International Journal of Radiation Oncology, Biology, Physics

DOI:
10.1016/j.ijrobp.2021.04.009

Publication date:
2021

Title Page (WITH Author Details)

Fractionated radiation severely reduces the number of CD8$^+$ T cells and mature antigen presenting cells within lung tumors

E. Reijmen[1], S. De Mey[2], W. De Mey[1], T. Gevaert[2], K. De Ridder[1], H. Locy[1], S. Martens[3], E. De Blay[4], L. Bouwens[4], P. Debie[5], K. Breckpot[1], J. De Grève[3], M. De Ridder[2], *C. Goyvaerts[1]

(1) Laboratory of Molecular and Cellular Therapy (LMCT), Department of Biomedical Sciences, Vrije Universiteit Brussel, Brussels, Belgium

(2) Department of Radiotherapy, Oncologisch Centrum, UZ Brussel, Vrije Universiteit Brussels, Brussels, Belgium

(3) Laboratory of Medical and Molecular Oncology (LMMO) and department of Medical Genetics, UZ Brussel, Brussels, Belgium

(4) Cell Differentiation Lab, Vrije Universiteit Brussel, Brussels, Belgium

(5) In vivo Cellular and Molecular Imaging laboratory, Vrije Universiteit Brussel, 1090 Brussels, Belgium

***Corresponding Author:**

Cleo Goyvaerts, Ph.D. Vrije Universiteit Brussel, Department of Biomedical Sciences, Laboratory for Molecular and Cellular Therapy, Laarbeeklaan 103, D, 1090 Jette, Belgium; Phone: 00324774573; E-mail: cleo.goyvaerts@vub.be

Conflicts of interest statement:

The authors have declared that no conflict of interest exists.

Funding information:

This work was supported by research grants from Kom op Tegen Kanker (Stand up to Cancer) and Vrije Universiteit Brussel under the strategic research program scheme (grant SRP48).

Data Sharing Statement: All available data can be obtained by contacting the corresponding author.

Abstract

Purpose The combination of standard-of-care radiotherapy (RT) with immunotherapy is moving to the mainstream of non-small cell lung cancer (NSCLC) treatment. Multiple preclinical studies reported on the $CD8^+$ T cell stimulating properties of RT, resulting in abscopal therapeutic effects. A literature search demonstrates that most preclinical lung cancer studies applied subcutaneous lung tumor models. Hence in-depth immunological evaluation of clinically relevant RT in orthotopic lung cancer models is lacking.

Methods Here, we studied the therapeutic and immunological effects of low-dose fractionated RT on lungs from C57BL/6 mice, challenged two weeks before with firefly luciferase expressing Lewis Lung Carcinoma cells via the tail vein. Low-dose fractionation was represented by 4 consecutive daily fractions of image-guided RT at 3.2 Gy.

Results We showed reduced lung tumor growth upon irradiation using *in vivo* bioluminescence imaging and immunohistochemistry. Moreover, significant immunological RT-induced changes were observed in irradiated lungs as well as in the periphery (spleen and blood). First, a significant decrease in the number of $CD8^+$ T cells and trends towards more $CD4^+$ and regulatory T cells were seen upon RT in all evaluated tissues. Notably, only in the periphery the remaining $CD8^+$ T cells showed a more activated phenotype. In addition, a significant expansion of neutrophils and monocytes was observed upon RT locally and systemically. Locally, RT increased the influx of tumor-associated macrophages and conventional type 2 dendritic cells (DCs), while the alveolar macrophages and conventional type 1 DCs dramatically dropped. Functionally, these antigen presenting cells severely reduced their CD86 expression, suggestive for a reduced capacity to induce potent immunity.

Conclusion Our results imply that low-dose fractionated RT of tumor-bearing lung tissue shifts the immune cell balance towards an immature myeloid cell dominating profile. These data argue for myeloid cell repolarizing strategies to enhance the abscopal effects of fractionated RT-treated NSCLC patients.

Keywords

Radiotherapy, NSCLC, lymphocytes, suppressive myeloid cells, tumor microenvironment.

Introduction

Lung cancer represents the most common cause of cancer-related mortality worldwide, with an estimated 1.8 million deaths each year (1). There are two main subtypes of lung cancer: small cell lung cancer and non-small cell lung cancer (NSCLC), accounting for 15% and 85% respectively. During the last five years, immunotherapy has profoundly improved the outcome for advanced NSCLC patients. More specifically via immune checkpoint inhibition (ICI) therapy, targeting the immune suppressive pathway consisting of programmed death-1 (PD-1) and its ligand (PD-L1) (2). Interestingly, radiotherapy (RT) has been proposed as *in situ* vaccination strategy that could further enhance the efficacy of ICI in NSCLC (3, 4).

Indeed, a growing body of clinical studies are suggestive for an ameliorated disease outcome for advanced NSCLC patients when treated with RT in combination with ICI (5). While it is clear that ICI improves the outcome of chemoradiotherapy for locally advanced NSCLC, this may be an independent effect of both modalities. For example, in the PACIFIC study both progression free and overall survival improved after anti-PD-L1 consolidation therapy (durvalumab compared to placebo) of NSCLC patients (6). As no unpretreated chemoradiotherapy group was taken along, no conclusions could be drawn as to whether chemoradiotherapy ameliorated ICI therapy or not. Moreover, the first completed single-arm NICOLAS phase II trial on the efficacy of adding nivolumab concurrently to chemoradiotherapy for stage III NSCLC patients concluded that they were unable to confirm a 1-year progression free survival rate of $\geq$ 45% (7). While ICI with or without RT can result in complete cure of advanced NSCLC, a sobering 80% of patients does not show a durable benefit today, implying the need for additional strategies to maximize their separate and combined clinical benefit.

The rationale behind RTs' immune stimulating potential lies within its capacity to induce immunogenic tumor cell death, which enables antigen presenting cells (APCs) to prime a tumor-specific cytotoxic T cell (CTL)-mediated attack (8). This can result in immune-mediated tumor cell eradication at the irradiated site as well as in the periphery a.k.a. the abscopal effect of RT. In parallel, RT has also been linked to the induction of an immunosuppressive environment which could hinder an effective antitumor immune response, amongst others via an influx of myeloid-derived suppressor cells (MDSCs) both locally and systemically (9). These diverging immunological effects are attributable to the different cancer models and types, radiation doses, partial versus whole tumor radiation and the RT schedule (10, 11). For example, immunogenic cell death has been shown to increase with RT dose due to a dose-dependent upregulation of MHC-I molecules and antigen release by tumor cells (8). However, high single doses of irradiation (> 20 Gy) have also been linked to an increase in regulatory T cell (Treg) infiltration, resulting in only modest tumor control (12). When single high-dose RT was compared to hypofractionated radiation (8-12 Gy), only the latter induced abscopal therapeutic effects via systemic type I IFN-mediated immune activation in mice (13, 14). Single low-dose (< 5 Gy) and hyperfractionated RT regimens, have been shown to stimulate CTL-mediated antitumor immunity alone and in synergy with ICI (15–17).

A literature search demonstrates that most preclinical lung cancer studies applied subcutaneous lung tumor models. Hence in-depth immunological evaluation of clinically relevant RT in orthotopic lung cancer models is lacking. The latter are preferred over subcutaneous models to reflect the clinical scenario in which lung tumor cells progress and interact with their organ-defined microenvironment (18, 19). Therefore, we applied a murine metastatic luciferase^{+} Lewis Lung Carcinoma (LLC) model to understand the therapeutic and pulmonary immunological outcome of clinically relevant low-dose (3.2 Gy) fractionated RT.

Materials & Methods

Mice and cell lines

Six- to eight-week old female C57BL/6 mice were purchased from Charles River (L'Abresle, France). All mice were kept under pathogen-free conditions in individually ventilated cages. The animal experiments were authorized by the Ethical Committee for laboratory animals of the Vrije Universiteit Brussel and executed in accordance to the European guidelines for animal experimentation (ethical dossier numbers: 18-281-8 and 20-214-14). Lewis lung carcinoma (LLC) cells were a gift from Prof. Dr. … (…). These cells were transduced with lentiviral vectors encoding firefly luciferase (transfer plasmid pDUAL_SFFV-Fluc_Ub-puroR) as previously described, resulting in LLC-Fluc cells allowing non-invasive lung foci growth evaluation using *in vivo* bioluminescence imaging (BLI). (20). These were maintained in Dulbecco's Modified Eagle's Medium (DMEM, Sigma-Aldrich) supplemented with 10% fetal bovine serum (FBS, Harlan), 100 units/mL penicillin, 100 µg/mL streptomycin and 2 mM L-Glutamine (Sigma-Aldrich) at 37°C, 5% CO_2, 21% O_2 and humidity level of 95%.

Murine tumor cell transfer and treatment

Mice (n=45) were injected intravenously with 5x1e5 LLC-Fluc cells dissolved in 200µL phosphate buffered saline (PBS, Sigma-Aldrich). Control mice were challenged with 200µL PBS only. Tumor progression was monitored by follow-up of body weight and *in vivo* BLI as described (21), starting one week after tumor challenge and shaving of the thorax skin. *In vivo* BLI was used to select and assign mice with similar photon counts to the RT treated or untreated control group.

Creation of 3D-printed mold

We designed a homemade 3D-printed mold to ensure positioning of the mice and dose-build-up (*Supplementary figure 1A*). Therefore, a CT scan (GE Revolution CT) was taken from a 6-week-old C57BL/6 mouse. Next, the CT images were transferred to the Ultimaker Cura program (Ultimaker Cura 4.8, Netherlands) for virtual 3D model construction. Finally, the mold

(18.5cm * 7cm * 3cm in size) was printed with polylactic acid (PLA) filaments using the Ultimaker Extended 2+ (Ultimaker). Via previous absolute dose measurements with an ionization chamber (data not shown), the HU values of these PLA filaments were found to approximate these of water within 1% to ensure a relevant buildup.

Radiation therapy planning

On day 8 after tumor challenge, a baseline pre-treatment CT scan was performed. Two mice were radiated with the same plan, so they underwent CT simulation per two to obtain radiation therapy planning CT images. Mice were anesthetized by intraperitoneal injection of an anesthetic Ketamine/Xylazine mix (87,5 mg/kg Ketamine (Ketamidor®, UK) and 12,5 mg/kg Xylazine (Rompun®, Germany) and immobilized in the 3D-printed mold (*Supplementary figure 1A*). CT images of 1 mm thickness were obtained and then transferred to the GE Advantage Windows software for contouring. Tumors were not visible on the CT images, so both lungs and heart were contoured on each CT image. Next planning target volumes (PTV) were generated for the lungs using Eclipse v15.6 (Varian Medical) with three fields at various gantry angles with an energy of 6MV at a dose rate of 600 monitor unit/min. Field size and multileaf collimator (MLC) were shaped to obtain the most suitable dose distribution to the lungs while minimizing low dose spread to the heart (*Supplementary figure 1B*). The planning objective was to deliver the prescription dose to > 99% of the PTV.

Radiation treatment process

Mice were treated using the Truebeam STx system (Varian, Palo Alto, CA, USA; BrainLAB AG, Feldkirchen, Germany). Starting from day 11, a total of 12.8 Gy in 4 fractions was given at 24-hour intervals. Before each treatment, mice were anesthetized and immobilized in the 3D-printed mold in the same manner as the CT simulation. Then, cone-beam CT images were obtained and registered with planning CT images. The necessary 6D shifts were sent to the couch and adjusted accordingly to the coordinate information derived from the matching CBCT and planning CT data. After adjustments, mice were treated with indicated doses.

In vivo bioluminescence imaging

In vivo bioluminescence imaging was performed 7 (pre-treatment) and 19 (post-treatment) days after LLC-Fluc tumor inoculation to assess lung tumor growth *in situ*. Mice were sedated via inhalation of Isoflo: 5% induction via inhalation and 2.5% maintenance, 2 minutes/mouse at an oxygen rate between 0.5 and 1.5 L/min. Five minutes before imaging, mice were injected intravenously with D-luciferin at 30mg/kg mouse body weight (Promega, Leiden, The Netherlands). Imaging was performed on a Biospace Photonimager and analyzed using M3 vision software as previously described (21).

Preparation of single cell suspensions

All mice underwent submandibular blood sampling at day 7 (baseline), day 13 (3 days after the first RT dose) and day 20 (5 days after the last dose of RT). Blood (200µL) was collected in heparin-coated tubes (Sarstedt, Germany), which were subsequently centrifuged for 10 minutes at 2000g to separate cell pellets from plasma, which was stored at -20°C for further analysis. Three weeks after tumor injection, mice were sacrificed by cervical dislocation under anesthesia (Isoflo) and death was confirmed by cessation of breathing and heartbeat. Next single cell suspensions from lung, axillary lymph nodes and spleen were prepared. Lungs were first perfused with 5mL PBS and transferred to 1ml Roswell Park Memorial Institute-1640 medium (RPMI-1640, Sigma-Aldrich) containing 300U/mL collagenase-I (Sigma-Aldrich). Tissues were cut to small pieces using scissors, incubated at 37°C for 45 minutes, and finally mechanically reduced using an 18G syringe until single cell suspensions could be passed through a 40µm strainer. Lymph nodes were incubated at 37°C for 30 minutes after their injection with 13IU/ml Liberase TL (Roche). Next lymph nodes were, like fresh spleens, transferred to 1mL PBS, stamped with the plunger of a 3cc syringe and passed through a 40µm strainer. Cell pellets from blood, lungs and spleens, were resuspended in 1ml of red blood cell lysis buffer, incubated for 5 minutes, followed by a centrifugation and wash step with PBS before further analysis.

Flow cytometry analysis

First, all cell pellets were incubated with eFluor506 Fixable Viability dye (Invitrogen) and CD16/32 antibody (BD Biosciences) to label death cells and block non-specific antibody binding respectively. Next, cell surface staining was performed for 30 minutes at 4°C in cold PBS containing 1% bovine serum albumin (BSA, Sigma-Aldrich) and 0.02% sodium azide (Sigma-Aldrich) (FACS buffer). Staining of surface markers was performed using the fluorescent-labeled antibodies listed in *Table 1.* The stained cells were evaluated on an LSRFortessa flow cytometer (Beckton Dickinson) while analysis was performed with the FlowJo 10.5.3 software (Tree Star Inc., Ashland, OR, USA).

Multiplex Luminex assay

Concentrations of cytokines, chemokines and growth factors were evaluated on 12,5μl of serum plasma sample *via* cytokine bead array technology. More specifically the Pro Mouse Chemokine Panel, 31-plex (BIO-RAD) was used to evaluate the following cytokines (CTACK, GM-CSF, IFN-γ, IL-1β, IL-2, IL-4, IL-6, IL-10, IL-16, TNF-α) and chemokines (BCA-1, ENA-78, Eotaxin(-2), Fractalkine, I-309, IP-10, I-TAC, KC, MCP-1, MCP-3, MCP-5, MDC, MIP-1α, MIP-1β, MIP-3α, RANTES, MIP-3β, SCYB16, SDF-1α, TARC). The procedure was performed according to the manufacturer's instructions.

Priming assay

Cell suspensions (3x1e5) from blood, spleen, draining lymph nodes (dLN) and lung tissue were cultured in 100 µl of complete RPMI medium with 30ng/ml recombinant IL-2 (Peprotech) in the presence of LLC cells (3x1e4). After 24 hours supernatants were collected for evaluation of IFN-γ secretion via a mouse IFN-γ ELISA kit from Invitrogen, in accordance with the manufacturer's guidelines. Cells were treated for an additional 4 hours with the protein transport inhibitor Golgi-stop (Monensin, BD Biosciences) prior to cell surface and intracellular staining for the detection of CD137 and IFN-γ positivity within $CD4^+$ and $CD8^+$ T lymphocytes.

Histology

The large left lobe of each murine lung was fixed in buffered 4% formaldehyde and paraffin embedded. Tissue sections of 4µm were deparaffinized, hydrated and stained with hematoxylin, eosin and saffron (HES). Next, tissue sections were dehydrated and mounted to allow histological evaluation. Immunohistochemistry images were acquired using a Leica DM 4000 microscope at 20x magnification.

Statistical Methods

Two-tailed unpaired t-tests were used to determine the significance of differences. A P value ≤ 0.0332 was used as the cut-off for significance. The asterisk number in the figures indicates the level of statistical significance as follows: * for $p < 0.05$; ** for $p < 0.01$; *** for $p < 0.001$ and **** for $p < 0.0001$. Aggregated data are presented in figures using mean values to represent the central tendency and standard error of the mean (SEM) to represent variability. All statistical analysis was computed using GraphPad Prism v 7.0.

Results

Lung tumor specific RT treatment results in tumor growth delay

In this study we aimed to explore the therapeutic and immunological outcome of clinically relevant low-dose (3,2 Gy) fractionated (4x) RT on whole lungs of mice bearing orthotopic syngeneic lung tumors. Previous studies indicate that lung tumor cells growing subcutaneously versus pulmonary induce different systemic immune effects (19). Therefore, we optimized a whole lung-restricted RT protocol for the treatment of metastatic murine LLC in which tumor cells undergo hematogenous spread to the lungs (*Figure 1A*). Orthotopic engraftment of firefly luciferase encoding LLC (LLC-Fluc) was assessed on day 7 to have allocate mice over the treatment control and RT group with equal distribution of photon counts. Anesthetized mice were positioned in a 3D-printed mold and subjected to CT scanning prior to RT to establish a tailored radiation field and locate organs at risk (*Figure 1B and Supplementary figure 1*). Tumor growth was compared between RT treated and untreated control mice using BLI and lung histology. We show significant RT-induced tumor growth delay, despite the early time point of analysis after treatment *(Figure 1C-F).*

RT results in a significant local and systemic $CD8^+$ T cell drop

The abundance of tumor infiltrated $CD8^+$ T cells is a good predictive marker for the efficacy of immunotherapies that rely on T cells for their tumor destroying properties in humans (22). As we want to decipher which clinically relevant immunological changes fractionated RT elicits, we first investigated the local and systemic abundance of the different T-cell populations: $CD45^+$ immune cells and $CD3^+$ T cells in general, next to $CD8^+$ CTLs, $CD4^+/CD25^-$ helper T and $CD25^+/CD127^-$ regulatory T (Treg) cell subsets (gating strategy depicted in *Figure 2A*). When we assessed the percentage of $CD45^+$ immune cells on day 20 after tumor inoculation in blood, spleen and lung tissue, we observed a significant decrease in spleen but not in blood nor lung in the irradiated mice compared to non-irradiated controls *(Figure 2B)*. Flow cytometry analysis further showed that RT significantly decreased the percentage of $CD3^+$ T lymphocytes

in lung (*Figure 2C, upper row)*, with similar trend in blood and spleen. This decrease was mainly attributable to the significant decrease of the $CD8^+$ subset in lung and spleen. In contrast, $CD4^+$ helper and Tregs cells showed a trend towards increased percentages in all evaluated organs within the RT group. NK cells form the innate counterpart of the adaptive CTLs and can express a wide range of activating and inhibitory receptors to directly target and kill cancer cells without the need for MHC specificity. We observed a systemic expansion of NK cells in blood and spleen after RT, while an opposite trend was seen within irradiated lung tissue *(Figure 2C, lower row)*.

To understand the functional assets of the remaining $CD8^+$ T cells, we co-cultured single-cell suspensions from tumor draining lymph nodes (dLNs), spleen and lung for 24hrs *in vitro* with LLC cells at a 10:1 ratio. While we observed a striking increase in the number of CD137/IFN-γ double positive $CD8^+$ T cells in dLN and spleen upon RT, a trend towards reduction of these double positive cells was observed in irradiated lung tissue derived single-cell suspensions *(Figure 2D)*. Similar trends were observed for the $CD4^+$ T cells (data not shown). In contrast, supernatants derived from irradiated lung tissue and not from spleen or dLNs, showed a significantly higher secretion of IFN-γ *(Figure 2E)*. These findings are not in line with the observed reduction in lung-derived IFN-γ^+ $CD4^+$ and 8^+ T cells and argue that alternative lung-specific cells are accountable for this RT-induced IFN-γ production. Additional validation for the suboptimal $CD8^+$ T cell activation state in irradiated lung tissue compared to the periphery, was found in their increased expression of the immune checkpoint and exhaustion marker PD-1 (*Figure 2F*).

Our results indicate that conformal tumor irradiation induces divergent effects on lymphocyte subsets. The $CD4^+$ subpopulation appears to be more radioresistant than the $CD8^+$ T lymphocytes and NK cells. While these numbers are suggestive for an overall unfavorable effector profile within irradiated lungs 5 days after RT, the latter does improve the peripheral activation status of the $CD3^+$ T cells.

RT treatment increases local and systemic suppressive myeloid subsets

Previously it has been shown that therapeutic radiation leads to local injury-like inflammation with a tumor specific increase in suppressive CD11b$^+$ myeloid cells (23). Our study confirms that fractionated RT of orthotopic LLC-bearing mice results in a significant rise in the number of CD11b$^+$ myeloid cells in blood, spleen and lung (*Figure 3B-D, first row*). Within the lung tumor microenvironment (TME) these myeloid cells are mainly represented by classical/inflammatory Ly6C$^+$ monocytes (IM, CD14$^+$ in human), non-classical/residential CX3CR1$^+$ Ly6C$^-$ monocytes (RM, CD16$^+$ in human), Ly6G$^+$ tumor associated neutrophils, SiglecF$^+$ alveolar macrophages (AMs), F4/80$^+$ tumor associated macrophages (TAMs) and dendritic cells (DCs) (24).

To understand which subsets were responsible for this systemic and local myeloid expansion, we first evaluated the monocytes (IM and RM in lung) and neutrophils, a.k.a. monocytic and granulocytic MDSCs, respectively. Circulating neutrophils increased during RT and were also raised in spleen and lung tissue 5 days after RT (*Figure 3B-D, second row*). The kinetic profile of the circulating Ly6C$^+$ IMs revealed that, in contrast to neutrophils, the number of IMs starts to increment only after RT treatment. Of note, in irradiated lung tissue not the increase of Ly6C$^+$ IMs but of Ly6C$^-$ RMs was most pronounced (*Figure 3B-D, third row*).

In several tumor models, RT induces recruitment of macrophages to the tumor site, irrespective of dose and fractionation regimen (25, 26). Our results confirm a significant increase in CD11b$^+$/CD11c$^-$/F4/80$^+$ TAMs (*Figure 4A*). In addition, we observed a trend towards more MHC-II^{hi} pro-inflammatory TAMs compared to MHC-II^{lo} immune-suppressive TAMs upon RT. In contrast, the percentage of Siglec-F$^+$/CD11c$^+$ alveolar macrophages (AM) significantly dropped within the lung upon RT treatment (*Figure 4B*).

The abundance of cross-presenting CD103$^+$ conventional type 1 DCs (cDC1) within tumors has been associated with NSCLC patient survival and appears critical for the success of ICI in preclinical models (27). We observed that cDC1 were significantly excluded from the TME upon RT, in contrast to a significant influx of CD11b$^+$ cDC2s (*Figure 4C*). Moreover, a significant decrease in the expression of CD86, linked to the maturation profile, could be

demonstrated in the different APC subsets (AM, TAM and DCs) within the lung TME *(Figure 4D)*. Finally, we identified (non-significant) plasma level alterations in four out of the 31 studied cytokines (CTACK, GM-CSF, IFN-γ, IL-1β, IL-2, IL-4, IL-6, IL-10, IL-16, TNF-α) and chemokines (BCA-1, ENA-78, Eotaxin(-2), Fractalkine, I-309, IP-10, I-TAC, KC, MCP-1, MCP-3, MCP-5, MDC, MIP-1α, MIP-1β, MIP-3α, RANTES, MIP-3β, SCYB16, SDF-1α, TARC) in blood of mice, 3 days after the first RT fraction. The results indicate that the chemokines granulocyte-macrophage colony-stimulating factor (GM-CSF), monocyte chemoattractant protein-1 (MCP-1) and the cytokine IL-10 increased, while blood levels of IL-6 slightly decreased. (*Figure 4E).*

Discussion

The impact of fractionated RT on immune function is widely agreed to be significant, yet systemic antitumor immunity outside the irradiated lung tumor field, termed the abscopal effect, remains rare in NSCLC patients. This lack of abscopal effect is not well understood, particularly in the context of low-dose fractionated RT of lung tumors, the most common regimen used in clinical practice. In the current study, we aimed to define local and systemic clinically relevant fractionated (4 x 3.2 Gy) RT-induced immunological changes using an orthotopic murine lung tumor model.

It has been reported that limited size T-cell infiltrated tumors respond better to ICI than large tumor volumes (28). Moreover, lymphopenia has been reported to be a poor prognostic factor in NSCLC patients treated with immunotherapy (29). We could demonstrate a significant ablative effect of fractionated RT on the $CD8^+$ T cells with a slight increased level of $CD25^+/CD127^-$ Tregs and PD-1^+ T cells. In combination with a decreased percentage of CD137/IFN-γ $double^+$ T cells, these findings are suggestive for a local suboptimal T cell activation profile for ICI upon RT.

As RT did result in significant tumor load reduction, the question arises to what degree the negative effect on CTLs mitigates an optimal abscopal response to RT. Dovedi et al. previously showed that low-dose fractionated RT does result in increased T cell infiltration next to enhanced expression of PD-L1 on tumor cells and neutrophils as a result of $CD8^+$ T cell activation and IFN-γ secretion (30). In line with the latter study, we also observed a significant increase of IFN-γ secretion by lung-derived single cell suspensions following RT. However, while Dovedi et al. show that $CD8^+$ T cells were the predominant producers of IFN-γ, our data imply that $CD4^+$ nor $CD8^+$ T cells can be held responsible for this local IFN-γ increase. These findings highlight that additional research is needed to further elucidate the cellular IFN-γ sources upon local RT, which are most likely linked to other (innate) effector cells like NKT and $\gamma\delta$ T cells (31). Interestingly, RT treatment did enhance the percentage of IFN-γ and CD137 double positive $CD8^+$ T cells in spleen and dLNs. Therefore, we speculate that the peripheral lymphoid compartment can play a pivotal role in influencing the functional activity of effector T

cells prior to tumor infiltration. Main differences between the study by Dovedi and our study design, is the fractionation schedule (5 x 2 Gy or 3 x 8 Gy versus 4 x 3,2 Gy) next to the use of subcutaneously inoculated and irradiated tumor models. Nevertheless it should be noted that the groups of Illidge and Demaria have repeatedly shown a synergistic benefit of concomitant ICI with low-dose fractionated RT, so it remains to be evaluated if we can also demonstrate this benefit in our model (16, 32, 33).

Next to the lymphocytic changes, numerous preclinical studies using different murine models showed that low-dose fractionated RT schedules can have a detrimental effect on the TME in comparison to single dose and hypofractionation regimens, partially because of the recruitment of immune suppressive myeloid cells (25, 34–37). In line, we demonstrated that our low-dose fractionated RT regimen significantly increased the percentage of neutrophils and monocytes both locally and systemically. Moreover we found an increased trend of MCP-1 (CCL-2) and GM-CSF, known to be involved in the recruitment and suppressive functions of neutrophils, $Ly6C^+$ monocytes (IMs) and macrophages (38). While IMs are known to be recruited to the TME *via* CCL2 and aid in tumor progression and therapy resistance via differentiation towards suppressive TAMs and monocyte derived DCs, the role of the $CX3CR1^+$ $Ly6C^-$ RMs is less clear. Schmall et al., demonstrated that LLC tumor growth was impaired in CX3CR1 as well as in CCL2 knock out mice, suggesting that both RMs and IMs aid in lung tumor progression (39). A finding that is confirmed by the observation that suppressive myeloid cell targeting has been shown to increase the antitumor effects of RT, regardless of the RT scheme (9). Interestingly, we could demonstrate an RM specific increase within irradiated lung tissue. As RMs have been correlated with NK cell recruitment, this finding hints to a link with the significant rise in circulating and splenic NK cells in our model (24).

In addition, we show that conventional RT induced more $F4/80^+$ macrophages within the tumor bearing lungs, be it with a more pronounced increase in MHC-II^{hi} 'M1-like' pro-inflammatory TAMs than MHC-II^{lo} 'M2-like'anti-inflammatory TAMs. In accordance with our results, Prakash H. et al. reported that low-dose radiation treatment resulted in a switch from pro-tumorigenic to anti-tumorigenic TAMs (15, 26). Interestingly, the opposite effect has been seen with (single)

high-dose and hypofractionated radiation (40–42). What's more, dysregulation of macrophage activation has been implicated in radiation-related chronic inflammation ensued by pneumonitis and fibrosis (43). Consistent with one previous study, resident AMs were depleted following exposure to RT (44). As these AMs withhold a variety of protective functions (45), their depletion together with an increase in MHC-II^{lo} anti-inflammatory TAMs could contribute to the slumbering chronic inflammation process often observed in advanced stage NSCLC.

Finally, DCs play a crucial role in T cell activation after RT-induced damage in cancer cells resulting in potential abscopal effects. In our model, RT failed to drive the expansion of cross-presenting CD103^{+} cDC1s, described to be essential for the development of a productive tumor-specific CTL response (33). Notably, RT significantly increased the number of cDC2 in lung tumor bearing mice. Mouse and human cDC2 can perform cross-presentation of cell-associated antigens when stimulated under specific conditions, albeit less efficiently than cDC1 (46). Therefore, these elevated numbers of cDC2 represent an interesting therapeutic target. This is supported by the observation that tumor antigen delivery to cDC2 using anti-DCIR2 antibodies as a targeting vehicle conferred protection against murine melanoma (47). Moreover, it was shown in a subcutaneous LLC model that vaccination with cDC2 isolated from LLC tumors facilitated tumor control (48). Therefore, it is tempting to speculate that manipulation of these cells after RT, for instance through smart designed tumor antigen and adjuvant loaded nanoparticles that drain to the lung, could be the way forward to harness the immune system to eliminate residual cancer cells (49). All APC subsets evaluated (F4/80^{+} macrophages, AMs, cDC1 and cDC2) showed diminished expression of the CD86 maturation marker. Therefore, any APC subset targeting strategy should withhold the appropriate adjuvants to durably turn the tide of the irradiated TME.

Conclusive remarks

In this study, we provide a detailed overview of fractionated radiation-induced immune changes in lung tumor tissue, blood and spleen. In brief, a significant ablative effect was seen for the CD8^{+} T cells, AMs and cDC1s 5 days after RT while an influx of neutrophils, monocytes and

immature antigen-presenting cells was promoted. From the clinic we know that immunotherapy added to RT benefits patients with locally advanced lung cancer. It remains unclear however, whether focal RT could improve the efficacy of immunotherapy in advanced lung cancer as well. Our results are not in favor of using RT alone, if an abscopal effect is aspired to tackle metastatic disease. To maximize the therapeutic potential of RT as monotherapy as well as in combination with immunotherapy, further research with clinically relevant RT regimens and orthotopic models will be crucial to translate the encouraging findings from bench to bedside.

References

1. Bray F, Ferlay J, Soerjomataram I, *et al.* Global cancer statistics 2018: GLOBOCAN estimates of incidence and mortality worldwide for 36 cancers in 185 countries. *CA. Cancer J. Clin.* 2018.

2. Ribas A, Wolchok JD. Cancer immunotherapy using checkpoint blockade. *Science*. 2018;359:1350–1355.

3. Jagodinsky JC, Harari PM, Morris ZS. The Promise of Combining Radiation Therapy with Immunotherapy. *Int. J. Radiat. Oncol.* 2020.

4. Locy H, de Mey S, de Mey W, *et al.* Immunomodulation of the Tumor Microenvironment: Turn Foe Into Friend. *Front. Immunol.* 2018.

5. D'Andrea MA, Reddy GK. Systemic Immunostimulatory Effects of Radiation Therapy Improves the Outcomes of Patients with Advanced NSCLC Receiving Immunotherapy. *Am. J. Clin. Oncol. Cancer Clin. Trials*. 2020;43:218–228.

6. Antonia SJ, Villegas A, Daniel D, *et al.* Overall survival with durvalumab after chemoradiotherapy in stage III NSCLC. *N. Engl. J. Med.* 2018.

7. Peters S, Felip E, Dafni U, *et al.* Progression-free and overall survival for concurrent nivolumab with standard concurrent chemo-radiotherapy in locally advanced stage IIIA/B NSCLC: Results from the European Thoracic Oncology Platform NICOLAS phase II trial (ETOP 6-14). *J. Thorac. Oncol.* 2020;16:278–288.

8. Reits EA, Hodge JW, Herberts CA, *et al.* Radiation modulates the peptide repertoire, enhances MHC class I expression, and induces successful antitumor immunotherapy. *J. Exp. Med.* 2006;203:1259–1271.

9. Kang C, Jeong SY, Song SY, *et al.* The emerging role of myeloid-derived suppressor cells in radiotherapy. *Radiat. Oncol. J.* 2020;38:1–10.

10. Kanagavelu S, Gupta S, Wu X, *et al.* In Vivo Effects of Lattice Radiation Therapy on Local and Distant Lung Cancer: Potential Role of Immunomodulation . *Radiat. Res.* 2014;182:149–162.

11. Markovsky E, Budhu S, Samstein RM, *et al.* An anti-tumor immune response is evoked by partial-volume single dose radiation in two murine models. *Int J Radiat Oncol Biol Phys*. 2019;103:697–708.

12. Schaue D, Ratikan JA, Iwamoto KS, *et al.* Maximizing tumor immunity with fractionated radiation. *Int. J. Radiat. Oncol. Biol. Phys.* 2012;83:1306–1310.

13. Dewan MZ, Galloway AE, Kawashima N, *et al.* Fractionated but Not Single-Dose Radiotherapy Induces an Immune-Mediated Abscopal Effect when Combined with Anti-CTLA-4 Antibody. *Clin. Cancer Res.* 2009;15:5379–5388.

14. Burnette BC, Liang H, Lee Y, *et al.* The Efficacy of Radiotherapy Relies upon Induction of Type I Interferon-Dependent Innate and Adaptive Immunity. *Cancer Res.* 2011;71:2488–2496.

15. Klug F, Prakash H, Huber PE, *et al.* Low-Dose Irradiation Programs Macrophage Differentiation to an iNOS+/M1 Phenotype that Orchestrates Effective T Cell Immunotherapy. *Cancer Cell*. 2013;24:589–602.

16. Dovedi SJ, Cheadle EJ, Popple AL, *et al.* Cancer Therapy: Preclinical Fractionated Radiation Therapy Stimulates Antitumor Immunity Mediated by Both Resident and Infiltrating Polyclonal T-cell Populations when Combined with PD-1 Blockade. *Clin Cancer Res*. 2017;23:5514–5540.

17. Grapin M, Richard C, Limagne E, *et al.* Optimized fractionated radiotherapy with anti-PD-L1 and anti-TIGIT: a promising new combination. *J. Immunother. Cancer*. 2019;7.

18. Aktar R, Dietrich A, Tillber F, *et al.* Pre-clinical imaging for establishment and comparison of orthotopic non-small cell lung carcinoma: In search for models reflecting clinical scenarios. *Br. J. Radiol.* 2019;92.

19. Masuda J, Takayama E, Strober W, *et al.* Tumor growth limited to subcutaneous site vs tumor growth in pulmonary site exhibit differential effects on systemic immunities. *Oncol. Rep.* 2017.

20. Hastir J-F, Delbauve S, Larbanoix L, *et al.* Hepatocarcinoma induces a tumor necrosis factor-dependent Kupffer cell death pathway that favors its proliferation upon partial hepatectomy. *Front. Oncol.* 2020;10:1996.

21. Keyaerts M, Verschueren J, Bos TJ, *et al.* Dynamic bioluminescence imaging for quantitative tumour burden assessment using IV or IP administration of D: -luciferin: effect on intensity, time kinetics and repeatability of photon emission. *Eur. J. Nucl. Med. Mol. Imaging*. 2008;35:999–1007.

22. Pu X, Wu L, Su D, *et al.* Immunotherapy for non-small cell lung cancers: biomarkers for predicting responses and strategies to overcome resistance. *BMC Cancer*. 2018;18:1082.

23. Ostrand-Rosenberg S, Horn LA, Ciavattone NG. Radiotherapy both promotes and inhibits myeloid-derived suppressor cell function: Novel strategies for preventing the tumor-protective effects of radiotherapy. *Front. Oncol.* 2019;9.

24. Lavin Y, Kobayashi S, Leader A, *et al.* Innate Immune Landscape in Early Lung Adenocarcinoma by Paired Single-Cell Analyses. *Cell*. 2017;169:750-765.e17.

25. Vatner RE, Formenti SC. Myeloid-Derived Cells in Tumors: Effects of Radiation. *Semin. Radiat. Oncol.* 2015.

26. Prakash H, Klug F, Nadella V, *et al.* Low doses of gamma irradiation potentially modifies immunosuppressive tumor microenvironment by retuning tumor-associated macrophages: Lesson from insulinoma. *Carcinogenesis*. 2015.

27. Salmon H, Idoyaga J, Rahman A, *et al.* Expansion and Activation of CD103+ Dendritic Cell Progenitors at the Tumor Site Enhances Tumor Responses to Therapeutic PD-L1 and BRAF Inhibition. *Immunity*. 2016.

28. Zappasodi R, Merghoub T, Wolchok JD. Emerging Concepts for Immune Checkpoint Blockade-Based Combination Therapies. *Cancer Cell*. 2018;33:581–598.

29. Cho Y, Park S, Byun HK, *et al.* Impact of Treatment-Related Lymphopenia on Immunotherapy for Advanced Non-Small Cell Lung Cancer. *Int. J. Radiat. Oncol. Biol. Phys.* 2019.

30. Dovedi SJ, Illidge TM. The antitumor immune response generated by fractionated radiation therapy may be limited by tumor cell adaptive resistance and can be circumvented by PD-L1 blockade. *Oncoimmunology*. 2015.

31. Klose CSN, Artis D. Innate lymphoid cells control signaling circuits to regulate tissue-specific immunity. *Cell Res.* 2020;30:475–491.

32. Dovedi SJ, Adlard AL, Lipowska-Bhalla G, *et al.* Acquired resistance to fractionated radiotherapy can be overcome by concurrent PD-L1 blockade. *Cancer Res.* 2014.

33. Vanpouille-Box C, Alard A, Aryankalayil MJ, *et al.* DNA exonuclease Trex1 regulates radiotherapy-induced tumour immunogenicity. *Nat. Commun.* 2017.

34. Filatenkov A, Baker J, Mueller AMS, *et al.* Ablative tumor radiation can change the tumor immune cell microenvironment to induce durable complete remissions. *Clin. Cancer Res.* 2015.

35. Lugade AA, Moran JP, Gerber SA, *et al.* Local Radiation Therapy of B16 Melanoma Tumors Increases the Generation of Tumor Antigen-Specific Effector Cells That Traffic to the Tumor. *J. Immunol.* 2005.

36. Ahn G-O, Tseng D, Liao C-H, *et al.* Inhibition of Mac-1 (CD11b/CD18) enhances tumor response to radiation by reducing myeloid cell recruitment. *Proc. Natl. Acad. Sci.* 2010;107:8363–8368.

37. Lan J, Li R, Yin LM, *et al.* Targeting Myeloid-derived Suppressor Cells and Programmed Death Ligand 1 Confers Therapeutic Advantage of Ablative Hypofractionated Radiation Therapy Compared With Conventional Fractionated Radiation Therapy. *Int. J. Radiat. Oncol. Biol. Phys.* 2018;101:74–87.

38. Wu C, Hua Q, Zheng L. Generation of Myeloid Cells in Cancer: The Spleen Matters. *Front. Immunol.* 2020;11:1126.

39. Schmall A, Al-Tamari HM, Herold S, *et al.* Macrophage and cancer cell cross-talk via CCR2 and CX3CR1 is a fundamental mechanism driving lung cancer. *Am. J. Respir. Crit. Care Med.* 2015;191:437–447.

40. Chiang CS, Fu SY, Wang SC, *et al.* Irradiation promotes an M2 macrophage phenotype in tumor hypoxia. *Front. Oncol.* 2012.

41. Okubo M, Kioi M, Nakashima H, *et al.* M2-polarized macrophages contribute to neovasculogenesis, leading to relapse of oral cancer following radiation. *Sci. Rep.* 2016.

42. Seifert L, Werba G, Tiwari S, *et al.* Radiation Therapy Induces Macrophages to Suppress T-Cell Responses Against Pancreatic Tumors in Mice. *Gastroenterology*. 2016.

43. Sunil SG, Raviraj R, Nagarajan D, *et al.* Radiation-induced lung injury: impact on macrophage dysregulation and lipid alteration–a review. *Immunopharmacol. Immunotoxicol.* 2019.

44. Groves AM, Johnston CJ, Misra RS, *et al.* Whole-Lung Irradiation Results in Pulmonary Macrophage Alterations that are Subpopulation and Strain Specific. *Radiat. Res.* 2015.

45. Allard B, Panariti A, Pernet E, *et al.* Novel protective role of alveolar macrophages in adaptation to lung injury. In: *European Respiratory Journal*.Vol 50. European Respiratory Society (ERS); 2017:PA340.

46. Vu Manh TP, Bertho N, Hosmalin A, *et al.* Investigating evolutionary conservation of dendritic cell subset identity and functions. *Front. Immunol.* 2015.

47. Neubert K, Lehmann CHK, Heger L, *et al.* Antigen Delivery to CD11c + CD8 − Dendritic Cells Induces Protective Immune Responses against Experimental Melanoma in Mice In Vivo . *J. Immunol.* 2014.

48. Laoui D, Keirsse J, Morias Y, *et al.* The tumour microenvironment harbours ontogenically distinct dendritic cell populations with opposing effects on tumour immunity. *Nat. Commun.* 2016.

49. Dewitte H, Verbeke R, Breckpot K, *et al.* Nanoparticle design to induce tumor immunity and challenge the suppressive tumor microenvironment. *Nano Today*. 2014.

Figure 1: Study design and therapeutic impact of RT. (A) Schematic overview of the study design. Twenty-two C57BL/6 mice were injected intravenously (i.v.) with $5x10^5$ firefly-luciferase expressing LLC (LLC-Fluc). Seven days later, bioluminescence imaging (BLI) data were used to allocate all mice in two groups: a treatment control and RT group, with an equal sum of photon counts in both groups. Four days later, mice were treated with RT delivered in four consecutive daily fractions of 3.2 Gy. Blood samples were isolated before treatment (baseline, day 7), 3 days after the first RT dose (day 13) and 5 days after the last dose of RT (day 20). On day 20 after tumor injection, mice were euthanized to collect perfused lungs and spleens. (**B**) RT treatment plan of anesthetized mice positioned in a 3D-printed mold. (**C**) On day 7 and 19, lung tumors were evaluated using *in vivo* BLI. Images of two animals from both treatment groups on day 7 (upper row) and day 19 (lower row) are shown with the integrated light signal of 7 minutes at peak activity. ***(D)*** The relative increase in bioluminescence was calculated as the proportion of bioluminescence (photon counts) at day 19 to day 7 (baseline counts). ***(E)*** HES-stained paraffin-embedded tumor samples were analyzed for tumor growth. ***(F)*** Measured nodule volume is shown as percentage (%) of total lung volume. Data are shown as mean ± SD of n=13 (RT) and n=9 (control). *P < 0,0332; ** 0,0021; *** 0,0002; **** 0,0001 by two-tailed unpaired t-tests.

Figure 2: Assessment of lymphoid populations in lung tumor bearing mice, treated with RT. **(A)** Gating strategy for lymphoid immune cell subsets. **(B)** Percentage of $CD45^+$ immune cells within viable gated singlets of blood, spleen and lung tissue, isolated 5 days after the last RT treatment. **(C)** Lymphoid percentage analysis of the $CD3^+$ T cells (within the $CD45^+$ immune population), $CD8^+$ T cells, $CD4^+$ effector T cells, $CD4^+/CD25^+/CD127^-$ Tregs (within the $CD3^+$ lymphoid fraction) and $CD45^+/CD19^-/CD3^-/CD56^+$ NK cells in blood, spleen and lung. **(D)** Gating scheme for and percentages of CD137 and IFN-γ double positive primary $CD45^+$ $CD8^+$ T cells derived from dLN, spleen and lung, after a 24hr co-cultivation period with LLC cells *in vitro*. **(E)** IFN-γ protein levels were evaluated via ELISA on the supernatants of dLN, spleen and lung tissue derived single-cell suspensions after a 24hr *in vitro* priming period. **(F)** Flow cytometry analysis of PD-1 expression (depicted as absolute counts representative for the mean fluorescence intensity) within the $CD8^+$ T cell fraction from isolated blood, spleen and lung tissue. Data represent three pooled experiments. Data are shown as mean ± SD of n=13 (RT) and n=9 (control). *P < 0,0332; ** 0,0021; *** 0,0002; **** 0,0001 by two-tailed unpaired t-tests.

Figure 3: Evaluation of monocytes and neutrophils in lung tumor bearing mice treated with RT. (A) Gating strategy for $CD11b^+/Ly6G^+$ neutrophils and $CD11b^+/MHCII^-/Ly6C^+$ inflammatory monocytes (IM). Moreover, the residential monocytes (RM) in lung tissue were gated as follows: $CD11b^+/MHCII^-/CD11c^+$. ***(B)*** Flow cytometry analyses of $CD11b^+$, $Ly6G^+$ and/or $Ly6C^+$ myeloid cells in blood before, during and 5 days after RT. ***(C)*** Flow cytometry analyses of $CD11b^+$, $Ly6G^+$ and/or $Ly6C^+$ myeloid cells five days after RT in spleen. ***(D)*** Flow cytometry analyses of $CD11b^+$, $Ly6G^+$ and/or $Ly6C^{+and/or-}$ myeloid cells five days after RT in lung respectively. Data from B-D

represent three pooled experiments. Data are shown as mean ± SD of n=13 (RT) *and n=9 (control). *P < 0,0332; ** 0,0021; *** 0,0002; **** 0,0001 by two-tailed unpaired t-tests.*

Figure 4: (A)** Quantitative analysis of TAMs and the proportion of MHCII^{hi}, MHCII^{lo} and **(B)** resident alveolar macrophages. **(C)** Lung percentages of CD103^{+} (cDC1) and CD103- (cDC2) gated on DCs were quantified and **(D)** MFI was calculated for their activating CD86 marker. **(E)**The change of expressed plasma cytokines during RT.* Data represent three pooled experiments. Data are shown as mean ± SD of n=13 (RT) and n=9 (control). *P < 0,0332; ** 0,0021; *** 0,0002; * 0,0001 by two-tailed unpaired t-tests.

***Supplementary figure 1: Setup of whole lung radiation of C57BL/6 mice. (A)** Image of sedated mouse positioned in a 3D-printed mold prior to radiation. **(B)** For accurate dose calculation of the whole lung region specifically, a planning CT with slice thickness of 1 mm was performed. Lungs, heart and tumor were contoured prior to Eclipse v15.6 (Varian) export. A high definition multileaf collimator (HD-MLC) system with leaves of 2.5 mm was used to conformally shape the 6MV beam. The figure shows the intended dose distribution to cover the tumor volume.*

Abstract

Purpose The combination of standard-of-care radiotherapy (RT) with immunotherapy is moving to the mainstream of non-small cell lung cancer (NSCLC) treatment. Multiple preclinical studies reported on the $CD8^+$ T cell stimulating properties of RT, resulting in abscopal therapeutic effects. A literature search demonstrates that most preclinical lung cancer studies applied subcutaneous lung tumor models. Hence in-depth immunological evaluation of clinically relevant RT in orthotopic lung cancer models is lacking.

Methods Here, we studied the therapeutic and immunological effects of low-dose fractionated RT on lungs from C57BL/6 mice, challenged two weeks before with firefly luciferase expressing Lewis Lung Carcinoma cells via the tail vein. Low-dose fractionation was represented by 4 consecutive daily fractions of image-guided RT at 3.2 Gy.

Results We showed reduced lung tumor growth upon irradiation using *in vivo* bioluminescence imaging and immunohistochemistry. Moreover, significant immunological RT-induced changes were observed in irradiated lungs as well as in the periphery (spleen and blood). First, a significant decrease in the number of $CD8^+$ T cells and trends towards more $CD4^+$ and regulatory T cells were seen upon RT in all evaluated tissues. Notably, only in the periphery the remaining $CD8^+$ T cells showed a more activated phenotype. In addition, a significant expansion of neutrophils and monocytes was observed upon RT locally and systemically. Locally, RT increased the influx of tumor-associated macrophages and conventional type 2 dendritic cells (DCs), while the alveolar macrophages and conventional type 1 DCs dramatically dropped. Functionally, these antigen presenting cells severely reduced their CD86 expression, suggestive for a reduced capacity to induce potent immunity.

Conclusion Our results imply that low-dose fractionated RT of tumor-bearing lung tissue shifts the immune cell balance towards an immature myeloid cell dominating profile. These data argue for myeloid cell repolarizing strategies to enhance the abscopal effects of fractionated RT-treated NSCLC patients.

Keywords

Radiotherapy, NSCLC, lymphocytes, suppressive myeloid cells, tumor microenvironment.

Introduction

Lung cancer represents the most common cause of cancer-related mortality worldwide, with an estimated 1.8 million deaths each year (1). There are two main subtypes of lung cancer: small cell lung cancer and non-small cell lung cancer (NSCLC), accounting for 15% and 85% respectively. During the last five years, immunotherapy has profoundly improved the outcome for advanced NSCLC patients. More specifically via immune checkpoint inhibition (ICI) therapy, targeting the immune suppressive pathway consisting of programmed death-1 (PD-1) and its ligand (PD-L1) (2). Interestingly, radiotherapy (RT) has been proposed as *in situ* vaccination strategy that could further enhance the efficacy of ICI in NSCLC (3, 4).

Indeed, a growing body of clinical studies are suggestive for an ameliorated disease outcome for advanced NSCLC patients when treated with RT in combination with ICI (5). While it is clear that ICI improves the outcome of chemoradiotherapy for locally advanced NSCLC, this may be an independent effect of both modalities. For example, in the PACIFIC study both progression free and overall survival improved after anti-PD-L1 consolidation therapy (durvalumab compared to placebo) of NSCLC patients (6). As no unpretreated chemoradiotherapy group was taken along, no conclusions could be drawn as to whether chemoradiotherapy ameliorated ICI therapy or not. Moreover, the first completed single-arm NICOLAS phase II trial on the efficacy of adding nivolumab concurrently to chemoradiotherapy for stage III NSCLC patients concluded that they were unable to confirm a 1-year progression free survival rate of $\geq$ 45% (7). While ICI with or without RT can result in complete cure of advanced NSCLC, a sobering 80% of patients does not show a durable benefit today, implying the need for additional strategies to maximize their separate and combined clinical benefit.

The rationale behind RTs' immune stimulating potential lies within its capacity to induce immunogenic tumor cell death, which enables antigen presenting cells (APCs) to prime a tumor-specific cytotoxic T cell (CTL)-mediated attack (8). This can result in immune-mediated tumor cell eradication at the irradiated site as well as in the periphery a.k.a. the abscopal effect of RT. In parallel, RT has also been linked to the induction of an immunosuppressive environment which could hinder an effective antitumor immune response, amongst others via an influx of myeloid-derived suppressor cells (MDSCs) both locally and systemically (9). These diverging immunological effects are attributable to the different cancer models and types, radiation doses, partial versus whole tumor radiation and the RT schedule (10, 11). For example, immunogenic cell death has been shown to increase with RT dose due to a dose-dependent upregulation of MHC-I molecules and antigen release by tumor cells (8). However, high single doses of irradiation (> 20 Gy) have also been linked to an increase in regulatory T cell (Treg) infiltration, resulting in only modest tumor control (12). When single high-dose RT was compared to hypofractionated radiation (8-12 Gy), only the latter induced abscopal therapeutic effects via systemic type I IFN-mediated immune activation in mice (13, 14). Single low-dose (< 5 Gy) and hyperfractionated RT regimens, have been shown to stimulate CTL-mediated antitumor immunity alone and in synergy with ICI (15–17).

A literature search demonstrates that most preclinical lung cancer studies applied subcutaneous lung tumor models. Hence in-depth immunological evaluation of clinically relevant RT in orthotopic lung cancer models is lacking. The latter are preferred over subcutaneous models to reflect the clinical scenario in which lung tumor cells progress and interact with their organ-defined microenvironment (18, 19). Therefore, we applied a murine metastatic luciferase^{+} Lewis Lung Carcinoma (LLC) model to understand the therapeutic and pulmonary immunological outcome of clinically relevant low-dose (3.2 Gy) fractionated RT.

Materials & Methods

Mice and cell lines

Six- to eight-week old female C57BL/6 mice were purchased from Charles River (L'Abresle, France). All mice were kept under pathogen-free conditions in individually ventilated cages. The animal experiments were authorized by the Ethical Committee for laboratory animals of the Vrije Universiteit Brussel and executed in accordance to the European guidelines for animal experimentation (ethical dossier numbers: 18-281-8 and 20-214-14). Lewis lung carcinoma (LLC) cells were a gift from Prof. Dr. … (…). These cells were transduced with lentiviral vectors encoding firefly luciferase (transfer plasmid pDUAL_SFFV-Fluc_Ub-puroR) as previously described, resulting in LLC-Fluc cells allowing non-invasive lung foci growth evaluation using *in vivo* bioluminescence imaging (BLI). (20). These were maintained in Dulbecco's Modified Eagle's Medium (DMEM, Sigma-Aldrich) supplemented with 10% fetal bovine serum (FBS, Harlan), 100 units/mL penicillin, 100 µg/mL streptomycin and 2 mM L-Glutamine (Sigma-Aldrich) at 37°C, 5% CO_2, 21% O_2 and humidity level of 95%.

Murine tumor cell transfer and treatment

Mice (n=45) were injected intravenously with 5x1e5 LLC-Fluc cells dissolved in 200µL phosphate buffered saline (PBS, Sigma-Aldrich). Control mice were challenged with 200µL PBS only. Tumor progression was monitored by follow-up of body weight and *in vivo* BLI as described (21), starting one week after tumor challenge and shaving of the thorax skin. *In vivo* BLI was used to select and assign mice with similar photon counts to the RT treated or untreated control group.

Creation of 3D-printed mold

We designed a homemade 3D-printed mold to ensure positioning of the mice and dose-build-up (*Supplementary figure 1A*). Therefore, a CT scan (GE Revolution CT) was taken from a 6-week-old C57BL/6 mouse. Next, the CT images were transferred to the Ultimaker Cura program (Ultimaker Cura 4.8, Netherlands) for virtual 3D model construction. Finally, the mold

(18.5cm * 7cm * 3cm in size) was printed with polylactic acid (PLA) filaments using the Ultimaker Extended 2+ (Ultimaker). Via previous absolute dose measurements with an ionization chamber (data not shown), the HU values of these PLA filaments were found to approximate these of water within 1% to ensure a relevant buildup.

Radiation therapy planning

On day 8 after tumor challenge, a baseline pre-treatment CT scan was performed. Two mice were radiated with the same plan, so they underwent CT simulation per two to obtain radiation therapy planning CT images. Mice were anesthetized by intraperitoneal injection of an anesthetic Ketamine/Xylazine mix (87,5 mg/kg Ketamine (Ketamidor®, UK) and 12,5 mg/kg Xylazine (Rompun®, Germany) and immobilized in the 3D-printed mold (*Supplementary figure 1A*). CT images of 1 mm thickness were obtained and then transferred to the GE Advantage Windows software for contouring. Tumors were not visible on the CT images, so both lungs and heart were contoured on each CT image. Next planning target volumes (PTV) were generated for the lungs using Eclipse v15.6 (Varian Medical) with three fields at various gantry angles with an energy of 6MV at a dose rate of 600 monitor unit/min. Field size and multileaf collimator (MLC) were shaped to obtain the most suitable dose distribution to the lungs while minimizing low dose spread to the heart (*Supplementary figure 1B*). The planning objective was to deliver the prescription dose to > 99% of the PTV.

Radiation treatment process

Mice were treated using the Truebeam STx system (Varian, Palo Alto, CA, USA; BrainLAB AG, Feldkirchen, Germany). Starting from day 11, a total of 12.8 Gy in 4 fractions was given at 24-hour intervals. Before each treatment, mice were anesthetized and immobilized in the 3D-printed mold in the same manner as the CT simulation. Then, cone-beam CT images were obtained and registered with planning CT images. The necessary 6D shifts were sent to the couch and adjusted accordingly to the coordinate information derived from the matching CBCT and planning CT data. After adjustments, mice were treated with indicated doses.

In vivo bioluminescence imaging

In vivo bioluminescence imaging was performed 7 (pre-treatment) and 19 (post-treatment) days after LLC-Fluc tumor inoculation to assess lung tumor growth *in situ*. Mice were sedated via inhalation of Isoflo: 5% induction via inhalation and 2.5% maintenance, 2 minutes/mouse at an oxygen rate between 0.5 and 1.5 L/min. Five minutes before imaging, mice were injected intravenously with D-luciferin at 30mg/kg mouse body weight (Promega, Leiden, The Netherlands). Imaging was performed on a Biospace Photonimager and analyzed using M3 vision software as previously described (21).

Preparation of single cell suspensions

All mice underwent submandibular blood sampling at day 7 (baseline), day 13 (3 days after the first RT dose) and day 20 (5 days after the last dose of RT). Blood (200µL) was collected in heparin-coated tubes (Sarstedt, Germany), which were subsequently centrifuged for 10 minutes at 2000g to separate cell pellets from plasma, which was stored at -20°C for further analysis. Three weeks after tumor injection, mice were sacrificed by cervical dislocation under anesthesia (Isoflo) and death was confirmed by cessation of breathing and heartbeat. Next single cell suspensions from lung, axillary lymph nodes and spleen were prepared. Lungs were first perfused with 5mL PBS and transferred to 1ml Roswell Park Memorial Institute-1640 medium (RPMI-1640, Sigma-Aldrich) containing 300U/mL collagenase-I (Sigma-Aldrich). Tissues were cut to small pieces using scissors, incubated at 37°C for 45 minutes, and finally mechanically reduced using an 18G syringe until single cell suspensions could be passed through a 40µm strainer. Lymph nodes were incubated at 37°C for 30 minutes after their injection with 13IU/ml Liberase TL (Roche). Next lymph nodes were, like fresh spleens, transferred to 1mL PBS, stamped with the plunger of a 3cc syringe and passed through a 40µm strainer. Cell pellets from blood, lungs and spleens, were resuspended in 1ml of red blood cell lysis buffer, incubated for 5 minutes, followed by a centrifugation and wash step with PBS before further analysis.

Flow cytometry analysis

First, all cell pellets were incubated with eFluor506 Fixable Viability dye (Invitrogen) and CD16/32 antibody (BD Biosciences) to label death cells and block non-specific antibody binding respectively. Next, cell surface staining was performed for 30 minutes at 4°C in cold PBS containing 1% bovine serum albumin (BSA, Sigma-Aldrich) and 0.02% sodium azide (Sigma-Aldrich) (FACS buffer). Staining of surface markers was performed using the fluorescent-labeled antibodies listed in *Table 1.* The stained cells were evaluated on an LSRFortessa flow cytometer (Beckton Dickinson) while analysis was performed with the FlowJo 10.5.3 software (Tree Star Inc., Ashland, OR, USA).

Multiplex Luminex assay

Concentrations of cytokines, chemokines and growth factors were evaluated on 12,5μl of serum plasma sample *via* cytokine bead array technology. More specifically the Pro Mouse Chemokine Panel, 31-plex (BIO-RAD) was used to evaluate the following cytokines (CTACK, GM-CSF, IFN-γ, IL-1β, IL-2, IL-4, IL-6, IL-10, IL-16, TNF-α) and chemokines (BCA-1, ENA-78, Eotaxin(-2), Fractalkine, I-309, IP-10, I-TAC, KC, MCP-1, MCP-3, MCP-5, MDC, MIP-1α, MIP-1β, MIP-3α, RANTES, MIP-3β, SCYB16, SDF-1α, TARC). The procedure was performed according to the manufacturer's instructions.

Priming assay

Cell suspensions (3x1e5) from blood, spleen, draining lymph nodes (dLN) and lung tissue were cultured in 100 µl of complete RPMI medium with 30ng/ml recombinant IL-2 (Peprotech) in the presence of LLC cells (3x1e4). After 24 hours supernatants were collected for evaluation of IFN-γ secretion via a mouse IFN-γ ELISA kit from Invitrogen, in accordance with the manufacturer's guidelines. Cells were treated for an additional 4 hours with the protein transport inhibitor Golgi-stop (Monensin, BD Biosciences) prior to cell surface and intracellular staining for the detection of CD137 and IFN-γ positivity within $CD4^+$ and $CD8^+$ T lymphocytes.

Histology

The large left lobe of each murine lung was fixed in buffered 4% formaldehyde and paraffin embedded. Tissue sections of 4µm were deparaffinized, hydrated and stained with hematoxylin, eosin and saffron (HES). Next, tissue sections were dehydrated and mounted to allow histological evaluation. Immunohistochemistry images were acquired using a Leica DM 4000 microscope at 20x magnification.

Statistical Methods

Two-tailed unpaired t-tests were used to determine the significance of differences. A P value ≤ 0.0332 was used as the cut-off for significance. The asterisk number in the figures indicates the level of statistical significance as follows: * for $p < 0.05$; ** for $p < 0.01$; *** for $p < 0.001$ and **** for $p < 0.0001$. Aggregated data are presented in figures using mean values to represent the central tendency and standard error of the mean (SEM) to represent variability. All statistical analysis was computed using GraphPad Prism v 7.0.

Results

Lung tumor specific RT treatment results in tumor growth delay

In this study we aimed to explore the therapeutic and immunological outcome of clinically relevant low-dose (3,2 Gy) fractionated (4x) RT on whole lungs of mice bearing orthotopic syngeneic lung tumors. Previous studies indicate that lung tumor cells growing subcutaneously versus pulmonary induce different systemic immune effects (19). Therefore, we optimized a whole lung-restricted RT protocol for the treatment of metastatic murine LLC in which tumor cells undergo hematogenous spread to the lungs (*Figure 1A*). Orthotopic engraftment of firefly luciferase encoding LLC (LLC-Fluc) was assessed on day 7 to have allocate mice over the treatment control and RT group with equal distribution of photon counts. Anesthetized mice were positioned in a 3D-printed mold and subjected to CT scanning prior to RT to establish a tailored radiation field and locate organs at risk (*Figure 1B and Supplementary figure 1*). Tumor growth was compared between RT treated and untreated control mice using BLI and lung histology. We show significant RT-induced tumor growth delay, despite the early time point of analysis after treatment *(Figure 1C-F).*

RT results in a significant local and systemic $CD8^+$ T cell drop

The abundance of tumor infiltrated $CD8^+$ T cells is a good predictive marker for the efficacy of immunotherapies that rely on T cells for their tumor destroying properties in humans (22). As we want to decipher which clinically relevant immunological changes fractionated RT elicits, we first investigated the local and systemic abundance of the different T-cell populations: $CD45^+$ immune cells and $CD3^+$ T cells in general, next to $CD8^+$ CTLs, $CD4^+/CD25^-$ helper T and $CD25^+/CD127^-$ regulatory T (Treg) cell subsets (gating strategy depicted in *Figure 2A*). When we assessed the percentage of $CD45^+$ immune cells on day 20 after tumor inoculation in blood, spleen and lung tissue, we observed a significant decrease in spleen but not in blood nor lung in the irradiated mice compared to non-irradiated controls *(Figure 2B)*. Flow cytometry analysis further showed that RT significantly decreased the percentage of $CD3^+$ T lymphocytes

in lung (*Figure 2C, upper row)*, with similar trend in blood and spleen. This decrease was mainly attributable to the significant decrease of the $CD8^+$ subset in lung and spleen. In contrast, $CD4^+$ helper and Tregs cells showed a trend towards increased percentages in all evaluated organs within the RT group. NK cells form the innate counterpart of the adaptive CTLs and can express a wide range of activating and inhibitory receptors to directly target and kill cancer cells without the need for MHC specificity. We observed a systemic expansion of NK cells in blood and spleen after RT, while an opposite trend was seen within irradiated lung tissue *(Figure 2C, lower row)*.

To understand the functional assets of the remaining $CD8^+$ T cells, we co-cultured single-cell suspensions from tumor draining lymph nodes (dLNs), spleen and lung for 24hrs *in vitro* with LLC cells at a 10:1 ratio. While we observed a striking increase in the number of CD137/IFN-γ double positive $CD8^+$ T cells in dLN and spleen upon RT, a trend towards reduction of these double positive cells was observed in irradiated lung tissue derived single-cell suspensions *(Figure 2D)*. Similar trends were observed for the $CD4^+$ T cells (data not shown). In contrast, supernatants derived from irradiated lung tissue and not from spleen or dLNs, showed a significantly higher secretion of IFN-γ *(Figure 2E)*. These findings are not in line with the observed reduction in lung-derived IFN-γ^+ $CD4^+$ and 8^+ T cells and argue that alternative lung-specific cells are accountable for this RT-induced IFN-γ production. Additional validation for the suboptimal $CD8^+$ T cell activation state in irradiated lung tissue compared to the periphery, was found in their increased expression of the immune checkpoint and exhaustion marker PD-1 (*Figure 2F*).

Our results indicate that conformal tumor irradiation induces divergent effects on lymphocyte subsets. The $CD4^+$ subpopulation appears to be more radioresistant than the $CD8^+$ T lymphocytes and NK cells. While these numbers are suggestive for an overall unfavorable effector profile within irradiated lungs 5 days after RT, the latter does improve the peripheral activation status of the $CD3^+$ T cells.

RT treatment increases local and systemic suppressive myeloid subsets

Previously it has been shown that therapeutic radiation leads to local injury-like inflammation with a tumor specific increase in suppressive CD11b$^+$ myeloid cells (23). Our study confirms that fractionated RT of orthotopic LLC-bearing mice results in a significant rise in the number of CD11b$^+$ myeloid cells in blood, spleen and lung (*Figure 3B-D, first row*). Within the lung tumor microenvironment (TME) these myeloid cells are mainly represented by classical/inflammatory Ly6C$^+$ monocytes (IM, CD14$^+$ in human), non-classical/residential CX3CR1$^+$ Ly6C$^-$ monocytes (RM, CD16$^+$ in human), Ly6G$^+$ tumor associated neutrophils, SiglecF$^+$ alveolar macrophages (AMs), F4/80$^+$ tumor associated macrophages (TAMs) and dendritic cells (DCs) (24).

To understand which subsets were responsible for this systemic and local myeloid expansion, we first evaluated the monocytes (IM and RM in lung) and neutrophils, a.k.a. monocytic and granulocytic MDSCs, respectively. Circulating neutrophils increased during RT and were also raised in spleen and lung tissue 5 days after RT (*Figure 3B-D, second row*). The kinetic profile of the circulating Ly6C$^+$ IMs revealed that, in contrast to neutrophils, the number of IMs starts to increment only after RT treatment. Of note, in irradiated lung tissue not the increase of Ly6C$^+$ IMs but of Ly6C$^-$ RMs was most pronounced (*Figure 3B-D, third row*).

In several tumor models, RT induces recruitment of macrophages to the tumor site, irrespective of dose and fractionation regimen (25, 26). Our results confirm a significant increase in CD11b$^+$/CD11c$^-$/F4/80$^+$ TAMs (*Figure 4A*). In addition, we observed a trend towards more MHC-II^{hi} pro-inflammatory TAMs compared to MHC-II^{lo} immune-suppressive TAMs upon RT. In contrast, the percentage of Siglec-F$^+$/CD11c$^+$ alveolar macrophages (AM) significantly dropped within the lung upon RT treatment (*Figure 4B*).

The abundance of cross-presenting CD103$^+$ conventional type 1 DCs (cDC1) within tumors has been associated with NSCLC patient survival and appears critical for the success of ICI in preclinical models (27). We observed that cDC1 were significantly excluded from the TME upon RT, in contrast to a significant influx of CD11b$^+$ cDC2s (*Figure 4C*). Moreover, a significant decrease in the expression of CD86, linked to the maturation profile, could be

demonstrated in the different APC subsets (AM, TAM and DCs) within the lung TME *(Figure 4D)*. Finally, we identified (non-significant) plasma level alterations in four out of the 31 studied cytokines (CTACK, GM-CSF, IFN-γ, IL-1β, IL-2, IL-4, IL-6, IL-10, IL-16, TNF-α) and chemokines (BCA-1, ENA-78, Eotaxin(-2), Fractalkine, I-309, IP-10, I-TAC, KC, MCP-1, MCP-3, MCP-5, MDC, MIP-1α, MIP-1β, MIP-3α, RANTES, MIP-3β, SCYB16, SDF-1α, TARC) in blood of mice, 3 days after the first RT fraction. The results indicate that the chemokines granulocyte-macrophage colony-stimulating factor (GM-CSF), monocyte chemoattractant protein-1 (MCP-1) and the cytokine IL-10 increased, while blood levels of IL-6 slightly decreased. (*Figure 4E).*

Discussion

The impact of fractionated RT on immune function is widely agreed to be significant, yet systemic antitumor immunity outside the irradiated lung tumor field, termed the abscopal effect, remains rare in NSCLC patients. This lack of abscopal effect is not well understood, particularly in the context of low-dose fractionated RT of lung tumors, the most common regimen used in clinical practice. In the current study, we aimed to define local and systemic clinically relevant fractionated (4 x 3.2 Gy) RT-induced immunological changes using an orthotopic murine lung tumor model.

It has been reported that limited size T-cell infiltrated tumors respond better to ICI than large tumor volumes (28). Moreover, lymphopenia has been reported to be a poor prognostic factor in NSCLC patients treated with immunotherapy (29). We could demonstrate a significant ablative effect of fractionated RT on the $CD8^+$ T cells with a slight increased level of $CD25^+/CD127^-$ Tregs and PD-1^+ T cells. In combination with a decreased percentage of CD137/IFN-γ $double^+$ T cells, these findings are suggestive for a local suboptimal T cell activation profile for ICI upon RT.

As RT did result in significant tumor load reduction, the question arises to what degree the negative effect on CTLs mitigates an optimal abscopal response to RT. Dovedi et al. previously showed that low-dose fractionated RT does result in increased T cell infiltration next to enhanced expression of PD-L1 on tumor cells and neutrophils as a result of $CD8^+$ T cell activation and IFN-γ secretion (30). In line with the latter study, we also observed a significant increase of IFN-γ secretion by lung-derived single cell suspensions following RT. However, while Dovedi et al. show that $CD8^+$ T cells were the predominant producers of IFN-γ, our data imply that $CD4^+$ nor $CD8^+$ T cells can be held responsible for this local IFN-γ increase. These findings highlight that additional research is needed to further elucidate the cellular IFN-γ sources upon local RT, which are most likely linked to other (innate) effector cells like NKT and $\gamma\delta$ T cells (31). Interestingly, RT treatment did enhance the percentage of IFN-γ and CD137 double positive $CD8^+$ T cells in spleen and dLNs. Therefore, we speculate that the peripheral lymphoid compartment can play a pivotal role in influencing the functional activity of effector T

cells prior to tumor infiltration. Main differences between the study by Dovedi and our study design, is the fractionation schedule (5 x 2 Gy or 3 x 8 Gy versus 4 x 3,2 Gy) next to the use of subcutaneously inoculated and irradiated tumor models. Nevertheless it should be noted that the groups of Illidge and Demaria have repeatedly shown a synergistic benefit of concomitant ICI with low-dose fractionated RT, so it remains to be evaluated if we can also demonstrate this benefit in our model (16, 32, 33).

Next to the lymphocytic changes, numerous preclinical studies using different murine models showed that low-dose fractionated RT schedules can have a detrimental effect on the TME in comparison to single dose and hypofractionation regimens, partially because of the recruitment of immune suppressive myeloid cells (25, 34–37). In line, we demonstrated that our low-dose fractionated RT regimen significantly increased the percentage of neutrophils and monocytes both locally and systemically. Moreover we found an increased trend of MCP-1 (CCL-2) and GM-CSF, known to be involved in the recruitment and suppressive functions of neutrophils, $Ly6C^+$ monocytes (IMs) and macrophages (38). While IMs are known to be recruited to the TME *via* CCL2 and aid in tumor progression and therapy resistance via differentiation towards suppressive TAMs and monocyte derived DCs, the role of the $CX3CR1^+$ $Ly6C^-$ RMs is less clear. Schmall et al., demonstrated that LLC tumor growth was impaired in CX3CR1 as well as in CCL2 knock out mice, suggesting that both RMs and IMs aid in lung tumor progression (39). A finding that is confirmed by the observation that suppressive myeloid cell targeting has been shown to increase the antitumor effects of RT, regardless of the RT scheme (9). Interestingly, we could demonstrate an RM specific increase within irradiated lung tissue. As RMs have been correlated with NK cell recruitment, this finding hints to a link with the significant rise in circulating and splenic NK cells in our model (24).

In addition, we show that conventional RT induced more $F4/80^+$ macrophages within the tumor bearing lungs, be it with a more pronounced increase in MHC-II^{hi} 'M1-like' pro-inflammatory TAMs than MHC-II^{lo} 'M2-like'anti-inflammatory TAMs. In accordance with our results, Prakash H. et al. reported that low-dose radiation treatment resulted in a switch from pro-tumorigenic to anti-tumorigenic TAMs (15, 26). Interestingly, the opposite effect has been seen with (single)

high-dose and hypofractionated radiation (40–42). What's more, dysregulation of macrophage activation has been implicated in radiation-related chronic inflammation ensued by pneumonitis and fibrosis (43). Consistent with one previous study, resident AMs were depleted following exposure to RT (44). As these AMs withhold a variety of protective functions (45), their depletion together with an increase in MHC-II^{lo} anti-inflammatory TAMs could contribute to the slumbering chronic inflammation process often observed in advanced stage NSCLC.

Finally, DCs play a crucial role in T cell activation after RT-induced damage in cancer cells resulting in potential abscopal effects. In our model, RT failed to drive the expansion of cross-presenting CD103^{+} cDC1s, described to be essential for the development of a productive tumor-specific CTL response (33). Notably, RT significantly increased the number of cDC2 in lung tumor bearing mice. Mouse and human cDC2 can perform cross-presentation of cell-associated antigens when stimulated under specific conditions, albeit less efficiently than cDC1 (46). Therefore, these elevated numbers of cDC2 represent an interesting therapeutic target. This is supported by the observation that tumor antigen delivery to cDC2 using anti-DCIR2 antibodies as a targeting vehicle conferred protection against murine melanoma (47). Moreover, it was shown in a subcutaneous LLC model that vaccination with cDC2 isolated from LLC tumors facilitated tumor control (48). Therefore, it is tempting to speculate that manipulation of these cells after RT, for instance through smart designed tumor antigen and adjuvant loaded nanoparticles that drain to the lung, could be the way forward to harness the immune system to eliminate residual cancer cells (49). All APC subsets evaluated (F4/80^{+} macrophages, AMs, cDC1 and cDC2) showed diminished expression of the CD86 maturation marker. Therefore, any APC subset targeting strategy should withhold the appropriate adjuvants to durably turn the tide of the irradiated TME.

Conclusive remarks

In this study, we provide a detailed overview of fractionated radiation-induced immune changes in lung tumor tissue, blood and spleen. In brief, a significant ablative effect was seen for the CD8^{+} T cells, AMs and cDC1s 5 days after RT while an influx of neutrophils, monocytes and

immature antigen-presenting cells was promoted. From the clinic we know that immunotherapy added to RT benefits patients with locally advanced lung cancer. It remains unclear however, whether focal RT could improve the efficacy of immunotherapy in advanced lung cancer as well. Our results are not in favor of using RT alone, if an abscopal effect is aspired to tackle metastatic disease. To maximize the therapeutic potential of RT as monotherapy as well as in combination with immunotherapy, further research with clinically relevant RT regimens and orthotopic models will be crucial to translate the encouraging findings from bench to bedside.

References

1. Bray F, Ferlay J, Soerjomataram I, *et al.* Global cancer statistics 2018: GLOBOCAN estimates of incidence and mortality worldwide for 36 cancers in 185 countries. *CA. Cancer J. Clin.* 2018.

2. Ribas A, Wolchok JD. Cancer immunotherapy using checkpoint blockade. *Science*. 2018;359:1350–1355.

3. Jagodinsky JC, Harari PM, Morris ZS. The Promise of Combining Radiation Therapy with Immunotherapy. *Int. J. Radiat. Oncol.* 2020.

4. Locy H, de Mey S, de Mey W, *et al.* Immunomodulation of the Tumor Microenvironment: Turn Foe Into Friend. *Front. Immunol.* 2018.

5. D'Andrea MA, Reddy GK. Systemic Immunostimulatory Effects of Radiation Therapy Improves the Outcomes of Patients with Advanced NSCLC Receiving Immunotherapy. *Am. J. Clin. Oncol. Cancer Clin. Trials*. 2020;43:218–228.

6. Antonia SJ, Villegas A, Daniel D, *et al.* Overall survival with durvalumab after chemoradiotherapy in stage III NSCLC. *N. Engl. J. Med.* 2018.

7. Peters S, Felip E, Dafni U, *et al.* Progression-free and overall survival for concurrent nivolumab with standard concurrent chemo-radiotherapy in locally advanced stage IIIA/B NSCLC: Results from the European Thoracic Oncology Platform NICOLAS phase II trial (ETOP 6-14). *J. Thorac. Oncol.* 2020;16:278–288.

8. Reits EA, Hodge JW, Herberts CA, *et al.* Radiation modulates the peptide repertoire, enhances MHC class I expression, and induces successful antitumor immunotherapy. *J. Exp. Med.* 2006;203:1259–1271.

9. Kang C, Jeong SY, Song SY, *et al.* The emerging role of myeloid-derived suppressor cells in radiotherapy. *Radiat. Oncol. J.* 2020;38:1–10.

10. Kanagavelu S, Gupta S, Wu X, *et al.* In Vivo Effects of Lattice Radiation Therapy on Local and Distant Lung Cancer: Potential Role of Immunomodulation . *Radiat. Res.* 2014;182:149–162.

11. Markovsky E, Budhu S, Samstein RM, *et al.* An anti-tumor immune response is evoked by partial-volume single dose radiation in two murine models. *Int J Radiat Oncol Biol Phys*. 2019;103:697–708.

12. Schaue D, Ratikan JA, Iwamoto KS, *et al.* Maximizing tumor immunity with fractionated radiation. *Int. J. Radiat. Oncol. Biol. Phys.* 2012;83:1306–1310.

13. Dewan MZ, Galloway AE, Kawashima N, *et al.* Fractionated but Not Single-Dose Radiotherapy Induces an Immune-Mediated Abscopal Effect when Combined with Anti-CTLA-4 Antibody. *Clin. Cancer Res.* 2009;15:5379–5388.

14. Burnette BC, Liang H, Lee Y, *et al.* The Efficacy of Radiotherapy Relies upon Induction of Type I Interferon-Dependent Innate and Adaptive Immunity. *Cancer Res.* 2011;71:2488–2496.

15. Klug F, Prakash H, Huber PE, *et al.* Low-Dose Irradiation Programs Macrophage Differentiation to an iNOS+/M1 Phenotype that Orchestrates Effective T Cell Immunotherapy. *Cancer Cell*. 2013;24:589–602.

16. Dovedi SJ, Cheadle EJ, Popple AL, *et al.* Cancer Therapy: Preclinical Fractionated Radiation Therapy Stimulates Antitumor Immunity Mediated by Both Resident and Infiltrating Polyclonal T-cell Populations when Combined with PD-1 Blockade. *Clin Cancer Res*. 2017;23:5514–5540.

17. Grapin M, Richard C, Limagne E, *et al.* Optimized fractionated radiotherapy with anti-PD-L1 and anti-TIGIT: a promising new combination. *J. Immunother. Cancer*. 2019;7.

18. Aktar R, Dietrich A, Tillber F, *et al.* Pre-clinical imaging for establishment and comparison of orthotopic non-small cell lung carcinoma: In search for models reflecting clinical scenarios. *Br. J. Radiol.* 2019;92.

19. Masuda J, Takayama E, Strober W, *et al.* Tumor growth limited to subcutaneous site vs tumor growth in pulmonary site exhibit differential effects on systemic immunities. *Oncol. Rep.* 2017.

20. Hastir J-F, Delbauve S, Larbanoix L, *et al.* Hepatocarcinoma induces a tumor necrosis factor-dependent Kupffer cell death pathway that favors its proliferation upon partial hepatectomy. *Front. Oncol.* 2020;10:1996.

21. Keyaerts M, Verschueren J, Bos TJ, *et al.* Dynamic bioluminescence imaging for quantitative tumour burden assessment using IV or IP administration of D: -luciferin: effect on intensity, time kinetics and repeatability of photon emission. *Eur. J. Nucl. Med. Mol. Imaging*. 2008;35:999–1007.

22. Pu X, Wu L, Su D, *et al.* Immunotherapy for non-small cell lung cancers: biomarkers for predicting responses and strategies to overcome resistance. *BMC Cancer*. 2018;18:1082.

23. Ostrand-Rosenberg S, Horn LA, Ciavattone NG. Radiotherapy both promotes and inhibits myeloid-derived suppressor cell function: Novel strategies for preventing the tumor-protective effects of radiotherapy. *Front. Oncol.* 2019;9.

24. Lavin Y, Kobayashi S, Leader A, *et al.* Innate Immune Landscape in Early Lung Adenocarcinoma by Paired Single-Cell Analyses. *Cell*. 2017;169:750-765.e17.

25. Vatner RE, Formenti SC. Myeloid-Derived Cells in Tumors: Effects of Radiation. *Semin. Radiat. Oncol.* 2015.

26. Prakash H, Klug F, Nadella V, *et al.* Low doses of gamma irradiation potentially modifies immunosuppressive tumor microenvironment by retuning tumor-associated macrophages: Lesson from insulinoma. *Carcinogenesis*. 2015.

27. Salmon H, Idoyaga J, Rahman A, *et al.* Expansion and Activation of CD103+ Dendritic Cell Progenitors at the Tumor Site Enhances Tumor Responses to Therapeutic PD-L1 and BRAF Inhibition. *Immunity*. 2016.

28. Zappasodi R, Merghoub T, Wolchok JD. Emerging Concepts for Immune Checkpoint Blockade-Based Combination Therapies. *Cancer Cell*. 2018;33:581–598.

29. Cho Y, Park S, Byun HK, *et al.* Impact of Treatment-Related Lymphopenia on Immunotherapy for Advanced Non-Small Cell Lung Cancer. *Int. J. Radiat. Oncol. Biol. Phys.* 2019.

30. Dovedi SJ, Illidge TM. The antitumor immune response generated by fractionated radiation therapy may be limited by tumor cell adaptive resistance and can be circumvented by PD-L1 blockade. *Oncoimmunology*. 2015.

31. Klose CSN, Artis D. Innate lymphoid cells control signaling circuits to regulate tissue-specific immunity. *Cell Res.* 2020;30:475–491.

32. Dovedi SJ, Adlard AL, Lipowska-Bhalla G, *et al.* Acquired resistance to fractionated radiotherapy can be overcome by concurrent PD-L1 blockade. *Cancer Res.* 2014.

33. Vanpouille-Box C, Alard A, Aryankalayil MJ, *et al.* DNA exonuclease Trex1 regulates radiotherapy-induced tumour immunogenicity. *Nat. Commun.* 2017.

34. Filatenkov A, Baker J, Mueller AMS, *et al.* Ablative tumor radiation can change the tumor immune cell microenvironment to induce durable complete remissions. *Clin. Cancer Res.* 2015.

35. Lugade AA, Moran JP, Gerber SA, *et al.* Local Radiation Therapy of B16 Melanoma Tumors Increases the Generation of Tumor Antigen-Specific Effector Cells That Traffic to the Tumor. *J. Immunol.* 2005.

36. Ahn G-O, Tseng D, Liao C-H, *et al.* Inhibition of Mac-1 (CD11b/CD18) enhances tumor response to radiation by reducing myeloid cell recruitment. *Proc. Natl. Acad. Sci.* 2010;107:8363–8368.

37. Lan J, Li R, Yin LM, *et al.* Targeting Myeloid-derived Suppressor Cells and Programmed Death Ligand 1 Confers Therapeutic Advantage of Ablative Hypofractionated Radiation Therapy Compared With Conventional Fractionated Radiation Therapy. *Int. J. Radiat. Oncol. Biol. Phys.* 2018;101:74–87.

38. Wu C, Hua Q, Zheng L. Generation of Myeloid Cells in Cancer: The Spleen Matters. *Front. Immunol.* 2020;11:1126.

39. Schmall A, Al-Tamari HM, Herold S, *et al.* Macrophage and cancer cell cross-talk via CCR2 and CX3CR1 is a fundamental mechanism driving lung cancer. *Am. J. Respir. Crit. Care Med.* 2015;191:437–447.

40. Chiang CS, Fu SY, Wang SC, *et al.* Irradiation promotes an M2 macrophage phenotype in tumor hypoxia. *Front. Oncol.* 2012.

41. Okubo M, Kioi M, Nakashima H, *et al.* M2-polarized macrophages contribute to neovasculogenesis, leading to relapse of oral cancer following radiation. *Sci. Rep.* 2016.

42. Seifert L, Werba G, Tiwari S, *et al.* Radiation Therapy Induces Macrophages to Suppress T-Cell Responses Against Pancreatic Tumors in Mice. *Gastroenterology*. 2016.

43. Sunil SG, Raviraj R, Nagarajan D, *et al.* Radiation-induced lung injury: impact on macrophage dysregulation and lipid alteration–a review. *Immunopharmacol. Immunotoxicol.* 2019.

44. Groves AM, Johnston CJ, Misra RS, *et al.* Whole-Lung Irradiation Results in Pulmonary Macrophage Alterations that are Subpopulation and Strain Specific. *Radiat. Res.* 2015.

45. Allard B, Panariti A, Pernet E, *et al.* Novel protective role of alveolar macrophages in adaptation to lung injury. In: *European Respiratory Journal*.Vol 50. European Respiratory Society (ERS); 2017:PA340.

46. Vu Manh TP, Bertho N, Hosmalin A, *et al.* Investigating evolutionary conservation of dendritic cell subset identity and functions. *Front. Immunol.* 2015.

47. Neubert K, Lehmann CHK, Heger L, *et al.* Antigen Delivery to CD11c + CD8 − Dendritic Cells Induces Protective Immune Responses against Experimental Melanoma in Mice In Vivo . *J. Immunol.* 2014.

48. Laoui D, Keirsse J, Morias Y, *et al.* The tumour microenvironment harbours ontogenically distinct dendritic cell populations with opposing effects on tumour immunity. *Nat. Commun.* 2016.

49. Dewitte H, Verbeke R, Breckpot K, *et al.* Nanoparticle design to induce tumor immunity and challenge the suppressive tumor microenvironment. *Nano Today*. 2014.

Figure 1: Study design and therapeutic impact of RT. (A) Schematic overview of the study design. Twenty-two C57BL/6 mice were injected intravenously (i.v.) with $5x10^5$ firefly-luciferase expressing LLC (LLC-Fluc). Seven days later, bioluminescence imaging (BLI) data were used to allocate all mice in two groups: a treatment control and RT group, with an equal sum of photon counts in both groups. Four days later, mice were treated with RT delivered in four consecutive daily fractions of 3.2 Gy. Blood samples were isolated before treatment (baseline, day 7), 3 days after the first RT dose (day 13) and 5 days after the last dose of RT (day 20). On day 20 after tumor injection, mice were euthanized to collect perfused lungs and spleens. (**B**) RT treatment plan of anesthetized mice positioned in a 3D-printed mold. (**C**) On day 7 and 19, lung tumors were evaluated using *in vivo* BLI. Images of two animals from both treatment groups on day 7 (upper row) and day 19 (lower row) are shown with the integrated light signal of 7 minutes at peak activity. ***(D)*** The relative increase in bioluminescence was calculated as the proportion of bioluminescence (photon counts) at day 19 to day 7 (baseline counts). ***(E)*** HES-stained paraffin-embedded tumor samples were analyzed for tumor growth. ***(F)*** Measured nodule volume is shown as percentage (%) of total lung volume. Data are shown as mean ± SD of n=13 (RT) and n=9 (control). *P < 0,0332; ** 0,0021; *** 0,0002; **** 0,0001 by two-tailed unpaired t-tests.

Figure 2: Assessment of lymphoid populations in lung tumor bearing mice, treated with RT. **(A)** Gating strategy for lymphoid immune cell subsets. **(B)** Percentage of $CD45^+$ immune cells within viable gated singlets of blood, spleen and lung tissue, isolated 5 days after the last RT treatment. **(C)** Lymphoid percentage analysis of the $CD3^+$ T cells (within the $CD45^+$ immune population), $CD8^+$ T cells, $CD4^+$ effector T cells, $CD4^+/CD25^+/CD127^-$ Tregs (within the $CD3^+$ lymphoid fraction) and $CD45^+/CD19^-/CD3^-/CD56^+$ NK cells in blood, spleen and lung. **(D)** Gating scheme for and percentages of CD137 and IFN-γ double positive primary $CD45^+$ $CD8^+$ T cells derived from dLN, spleen and lung, after a 24hr co-cultivation period with LLC cells *in vitro*. **(E)** IFN-γ protein levels were evaluated via ELISA on the supernatants of dLN, spleen and lung tissue derived single-cell suspensions after a 24hr *in vitro* priming period. **(F)** Flow cytometry analysis of PD-1 expression (depicted as absolute counts representative for the mean fluorescence intensity) within the $CD8^+$ T cell fraction from isolated blood, spleen and lung tissue. Data represent three pooled experiments. Data are shown as mean ± SD of n=13 (RT) and n=9 (control). *P < 0,0332; ** 0,0021; *** 0,0002; **** 0,0001 by two-tailed unpaired t-tests.

Figure 3: Evaluation of monocytes and neutrophils in lung tumor bearing mice treated with RT. (A) Gating strategy for $CD11b^+/Ly6G^+$ neutrophils and $CD11b^+/MHCII^-/Ly6C^+$ inflammatory monocytes (IM). Moreover, the residential monocytes (RM) in lung tissue were gated as follows: $CD11b^+/MHCII^-/CD11c^+$. ***(B)*** Flow cytometry analyses of $CD11b^+$, $Ly6G^+$ and/or $Ly6C^+$ myeloid cells in blood before, during and 5 days after RT. ***(C)*** Flow cytometry analyses of $CD11b^+$, $Ly6G^+$ and/or $Ly6C^+$ myeloid cells five days after RT in spleen. ***(D)*** Flow cytometry analyses of $CD11b^+$, $Ly6G^+$ and/or $Ly6C^{+and/or-}$ myeloid cells five days after RT in lung respectively. Data from B-D

represent three pooled experiments. Data are shown as mean ± SD of n=13 (RT) *and n=9 (control). *P < 0,0332; ** 0,0021; *** 0,0002; **** 0,0001 by two-tailed unpaired t-tests.*

Figure 4: (A)** Quantitative analysis of TAMs and the proportion of MHCII^{hi}, MHCII^{lo} and **(B)** resident alveolar macrophages. **(C)** Lung percentages of CD103^{+} (cDC1) and CD103- (cDC2) gated on DCs were quantified and **(D)** MFI was calculated for their activating CD86 marker. **(E)**The change of expressed plasma cytokines during RT.* Data represent three pooled experiments. Data are shown as mean ± SD of n=13 (RT) and n=9 (control). *P < 0,0332; ** 0,0021; *** 0,0002; * 0,0001 by two-tailed unpaired t-tests.

***Supplementary figure 1: Setup of whole lung radiation of C57BL/6 mice. (A)** Image of sedated mouse positioned in a 3D-printed mold prior to radiation. **(B)** For accurate dose calculation of the whole lung region specifically, a planning CT with slice thickness of 1 mm was performed. Lungs, heart and tumor were contoured prior to Eclipse v15.6 (Varian) export. A high definition multileaf collimator (HD-MLC) system with leaves of 2.5 mm was used to conformally shape the 6MV beam. The figure shows the intended dose distribution to cover the tumor volume.*

Table 1: List of fluorescently labeled antibodies

	Marker	Clone	Fluorochrome	Dilution	Vendor
Systemic myeloid panel	CD45		BB515	200	BD
	CD11b	M1/70	AF700	100	Biolegend
	Ly6G	IA8	AF647	200	BD
	Ly6C		PE-Cy7	200	BD
	MHCII	M5/114.15.2	PE/Dazzle 594	600	Biolegend
	CD11c	N418	PerCPCy5.5	100	Biolegend
	B220		APC-eF780 (Cy7)	200	BD
	CD80		BV510	200	BD
Lung Myeloid panel	CD45.2	104 eBio	APC-eF780 (Cy7)	100	BD
	CD11b	M1/70	AF700	100	Biolegend
	Ly6G	IA8	AF647	200	BD
	Ly6C		PECy7	200	BD
	MHCII	M5/114.15.2	PE/Dazzle 594	600	Biolegend
	CD11c	N418	AF488	200	Biolegend
	Siglec-F	E50-2440	PE	200	BD
	CD103	M290	PerCPCy5.5	100	BD
	F4/80	BM8	PerCPCy5.5	100	Biolegend
	CD86	GL-1	BV605	200	Biolegend
Lymphoid panel	CD45		V450	100	BD
	CD3	145-2C11	PerCPCy5.5	100	Biolegend
	CD4	RM4-5	AF700	200	BD
	CD8	53-6.7	FITC	200	Biolegend
	CD19	1D3	AF647	100	BD
	CD25	PC61	BB515	200	BD
	CD127	SB/199	PE-CF594	200	BD
	PD1	J43	PE-Cy7	200	Invitrogen
	CD56	BV510	BV510	100	BD
Functional panel	CD45	104	APC-Cy7	200	BD
	CD3	17A2	AF488	200	Biolegend
	CD8	V450	53-6.7	200	BD
	CD4	RM4-5	AF700	200	BD
	CD137	17B5	PE	200	Biolegend
	IFN-γ	XMG1.2	PECy7	200	Biolegend
	IL-2	JES6-5H4	AF647	200	Biolegend

Figure

Click here to access/download;Figure;Figure 1 paper IJROBP.pptx

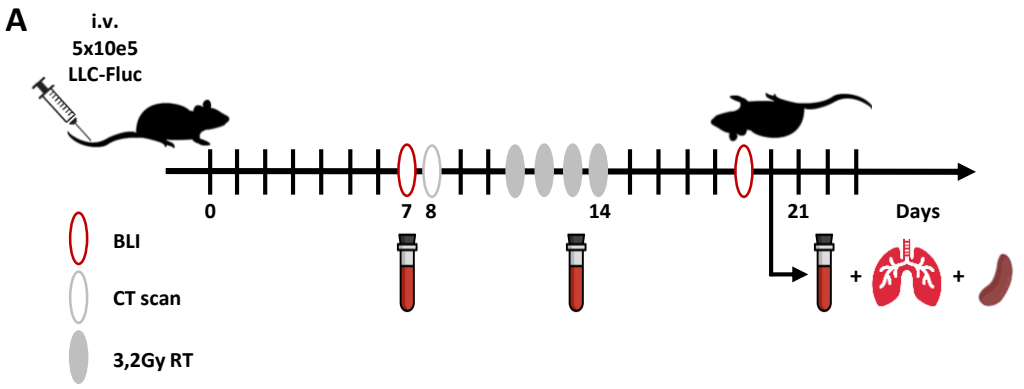

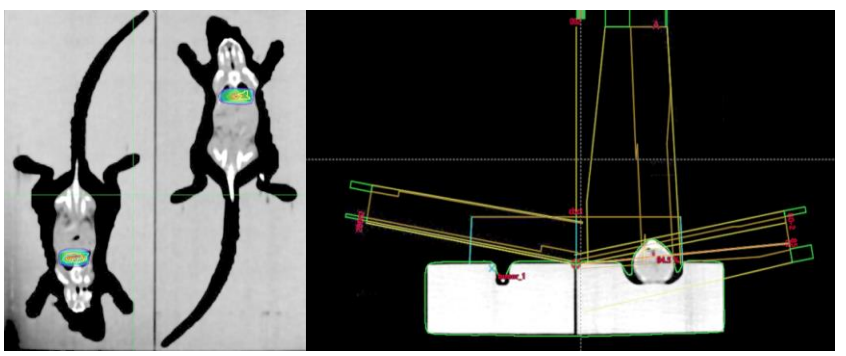

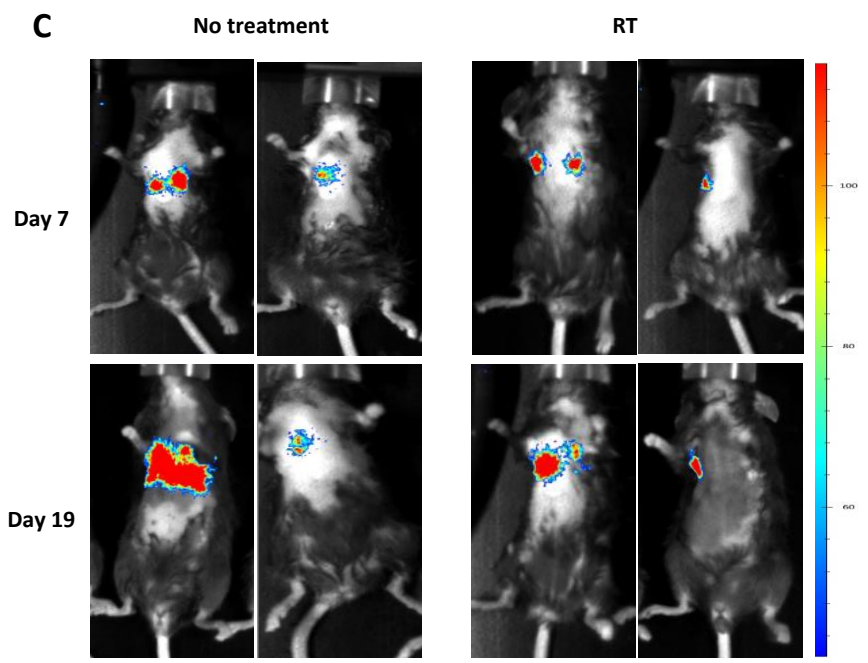

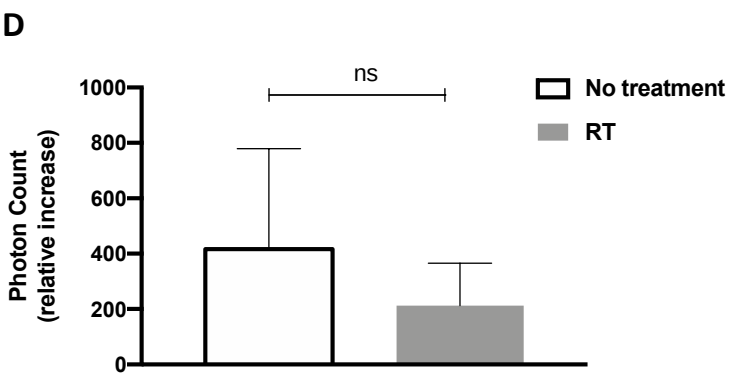

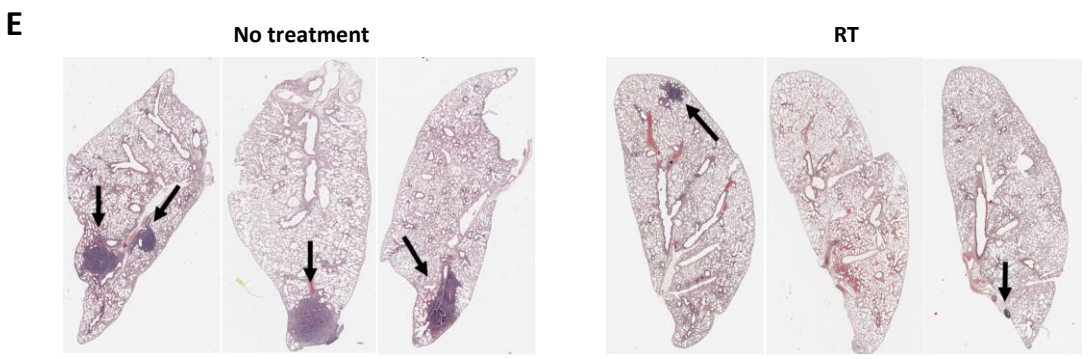

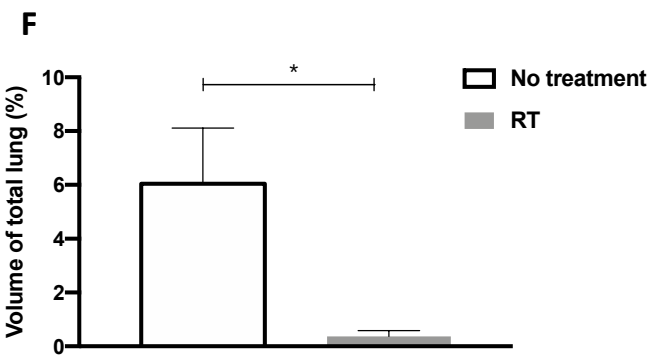

Figure

Click here to access/download;Figure;Figure 2 paper IJROBP.pptx

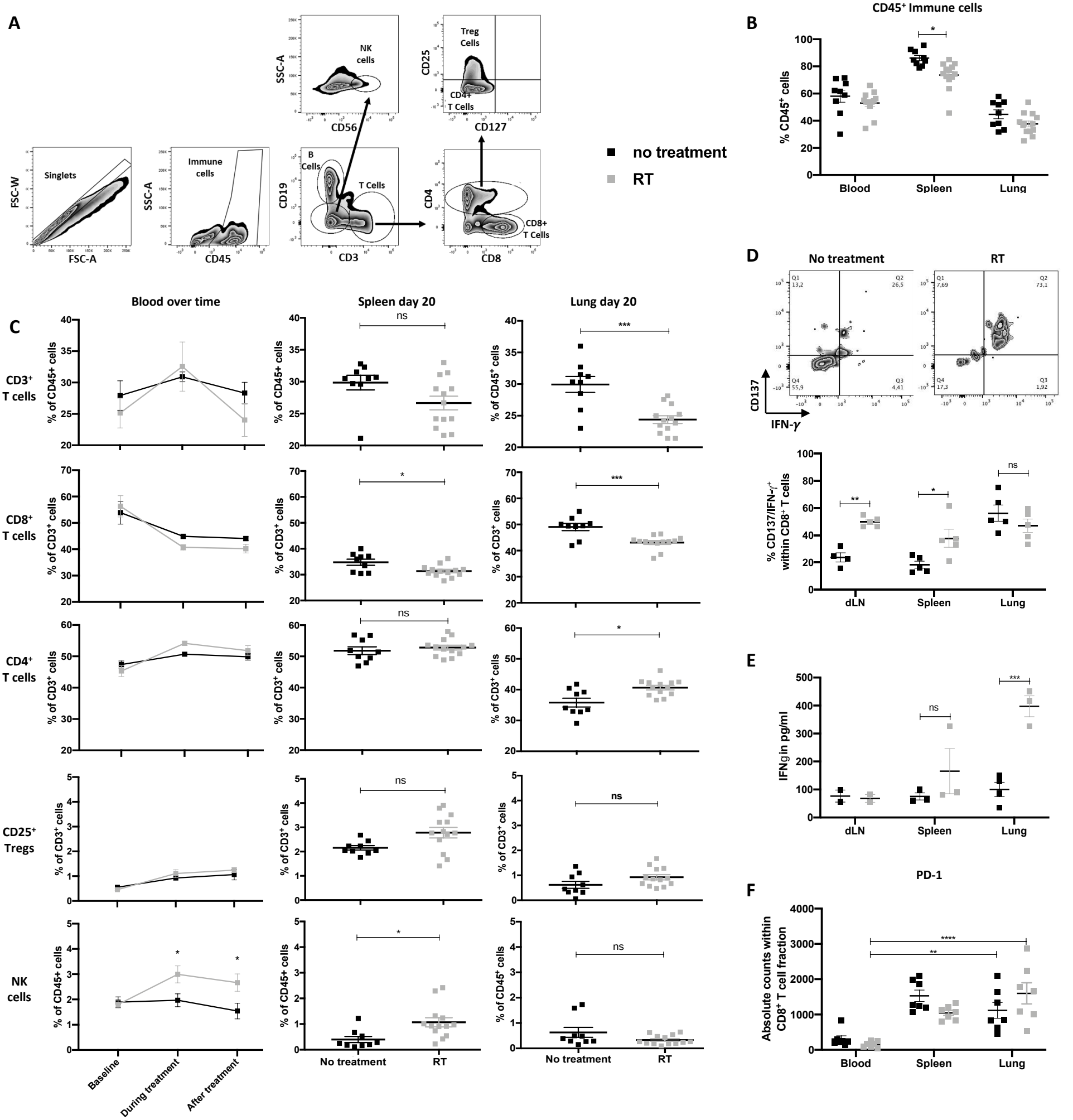

Figure

Click here to access/download;Figure;Figure 3 paper IJROBP.pptx

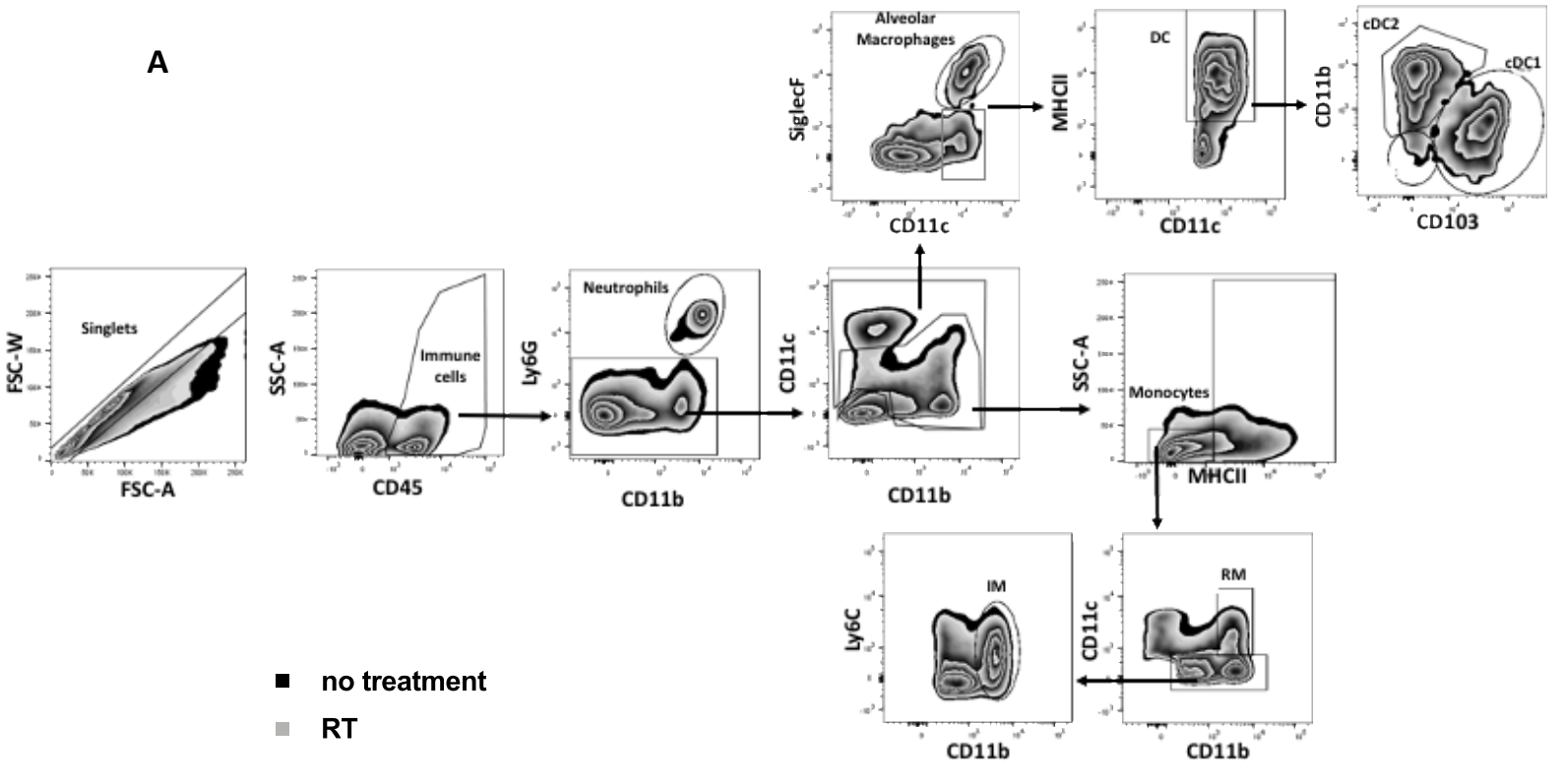

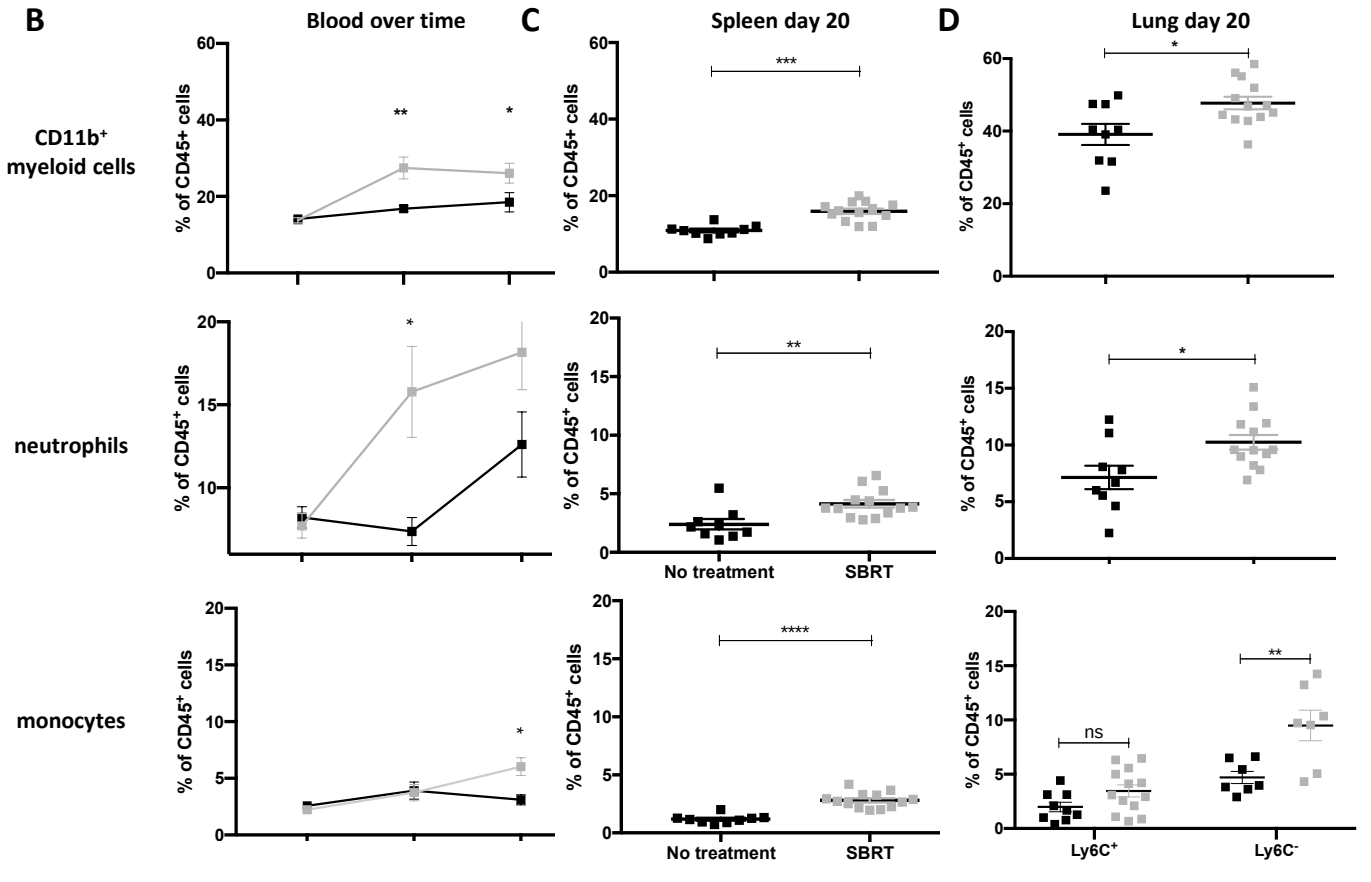

Figure

Click here to access/download;Figure;Figure 4 paper IJROBP.pptx